Delay Efficient FA-Assisted Satellite Communication Network with Mobile Edge Computing

Jingwen Zhao, Ming Chen, Zhaohui Yang, Hao Xu, Cunhua Pan, Tony Q.S. Quek, Kai-Kit Wong.

***Abstract*—Mobile edge computing–space-air-ground integrated network (MEC-SAGIN) is emerging as a crucial component of future wireless systems. Despite its potential, addressing network fluctuations while ensuring continuous low-latency computing services in highly dynamic environments remains a significant challenge. To address this issue, this paper proposes a fluid antenna (FA)-assisted MEC-SAGIN system, which enhances channel transmission conditions and reduces uplink task offloading latency by flexibly adjusting the antenna ports of edge computing users equipped with FAs. Specifically, we aim to minimize the maximum total computational delay (TCD) of edge computing tasks for ground users (GUs) and the satellite user (SU) by jointly optimizing the task offloading strategies, computational resource allocation, FA port positions, unmanned aerial vehicle (UAV) location, and the receive beamforming matrix. To solve this non-convex problem, we employ the block coordinate descent (BCD) technique to decompose the original problem into four subproblems. The subproblems are optimized using a combination of low-complexity iterative algorithms and the projected gradient descent (PGD) method to refine communication and computation configurations as well as FA port selection. Simulation results demonstrate that the FA-assisted scheme significantly improves the TCD performance of the MEC-SAGIN system. It maintains transmission stability and reliability in dynamic environments while outperforming conventional fixed-position antennas (FPAs) and random-port antenna schemes.**

***Index Terms*—Mobile edge computing, fluid antenna, satellite communication, unmanned aerial vehicle, resource allocation.**

I. Introduction

A. Motivation and Scope

With the rapid development of the sixth-generation (6G) mobile communication systems, the number of wireless devices worldwide is growing exponentially [1] [2]. However, the connection of large-scale wireless devices to a network results in the demand for services that require high bandwidth and computational resources [3] [4]. Mobile edge computing (MEC), as one of the emerging technologies in 5G, effectively reduces communication latency by migrating computational resources from centralized data centers to the edge of the network, thereby providing powerful support for latency-sensitive applications [5]–[8]. Nevertheless, there are still many challenges that MEC should address in practical applications, including the complexity of resource allocation, the quality of service assurance, and the coordination of multi-access technologies [9] [10]. These challenges constrain the scalable deployment of MEC, particularly in highly dynamic environments and large-scale user access scenarios.

In this context, the space-air-ground integrated network (SAGIN), as a promising architecture, has attracted significant attention from both academia and industry [11] [12]. By integrating satellite, unmanned aerial vehicle (UAV), and ground networks, SAGIN realizes seamless communication between air, space, and ground, demonstrating immense potential in application scenarios such as remote areas, post-disaster recovery, and wide-area coverage [13]. The deployment of SAGIN not only extends the coverage of communication networks through the coordinated scheduling and management of cross-domain resources but also enhances robustness and flexibility [14]. This facilitates new opportunities for the further advancement of MEC, establishing SAGIN as an effective solution to address challenges such as insufficient network coverage and communication latency.

Existing efforts have been made to achieve efficient communication and computation offloading in MEC-enabled SAGIN systems [15]–[17]. The existing literature primarily focuses on how to utilize the multi-layered network structure of SAGIN to enhance the computational and communication capabilities of MEC, such as by extending the coverage of edge computing through satellite networks or dynamically deploying computational resources via UAVs [18] [19]. Specifically, the works in [20]–[22] have explored various designs for uplink communication and computation offloading in SAGIN. Considering the services of MEC in the SAGIN system, ground users (GUs) can typically offload their computational tasks to edge servers on UAVs or satellites, thereby conserving energy and/or reducing computation latency for GUs [23]–[25]. Nonetheless, while existing studies have primarily concentrated on the distinct advantages of MEC and SAGIN networks, there remains a lack of in-depth research on the challenges arising from the integration of these two technologies in novel network architectures. These challenges include increased network complexity and the optimization of resources in dynamic environments. In particular, the communication among satellites, UAVs, and GUs within SAGIN is susceptible to multipath fading and link instability in highly dynamic environments, which imposes significant challenges on the offloading of computational tasks and resource allocation in MEC.

To address these challenges, the integration of fluid antenna (FA) technology has gradually emerged as a prominent solution [26]–[29]. By dynamically adjusting the antenna position within a constrained spatial domain, FAs can better exploit spatial diversity, thereby mitigating the impact of

J. Zhao, M. Chen, H. Xu and C. Pan are with the National Mobile Communications Research Laboratory, Southeast University, Nanjing 210096, China, email: {zhaojingwen, chenming, hao.xu, cpan}@seu.edu.cn.

Z. Yang is with the College of Information Science and Electronic Engineering, Zhejiang University, Hangzhou 310027, China, email: yang_zhaohui@zju.edu.cn.

Tony Q.S. Quek is with the Singapore University of Technology and Design, Singapore 487372, and also with the Yonsei Frontier Lab, Yonsei University, South Korea, email: tonyquek@sutd.edu.sg.

Kai-Kit Wong is with the Department of Electronic and Electrical Engineering, University College London, WC1E 7JE London, U.K., and also with the Yonsei Frontier Laboratory, Yonsei University, Seoul 03722, South Korea, e-mail: kai-kit.wong@ucl.ac.uk.

multipath fading on signal transmission [30]–[32]. Specifically, FA technology enables the adjustment of the antenna position vector (APV) and antenna weight vector (AWV) to achieve full array gain in the desired direction and interference nulling in multiple undesired directions [33] [34]. Compared to conventional fixed-position antennas (FPAs), FAs exhibit superior efficiency and adaptability, thus further improving the reliability and stability of the communication network [35] [36]. Recent studies have explored FAs in MEC and in SAGIN as two largely separate threads. Specifically, in MEC networks, the reconfigurability of FAs enables opportunistic port selection and position adaptation, which improves uplink signal-to-interference-plus-noise ratio (SINR), reduces the transmit power required for reliable offloading, and consequently shortens end-to-end latency [37] [38]. In SAGIN networks, FAs provide interference containment and adaptive beam footprints, while port diversity suppresses inter-beam leakage, which enhances link reliability under rapid geometric variation and Doppler effects, and thereby improves spectral reuse compared with fixed-pattern arrays [39]. However, these studies analyze the benefits of FAs within isolated MEC or SAGIN settings.

With FA technology already demonstrating its effectiveness in both MEC and SAGIN systems, as well as its adaptability to complex and dynamic environments, this technology serves as an effective solution for providing flexible adjustment capabilities to alleviate edge computing network congestion in high-speed SAGIN environments. Therefore, we propose to utilize FAs in the integrated MEC-SAGIN hybrid network to address the limitations of the existing network architectures. To the best of our knowledge, there is currently no research on the application of FA technology for enabling edge computing within SAGIN networks. To fill this research gap, we propose a novel SAGIN architecture that integrates satellite, UAV, GUs, and FA technology to enhance the stability and reliability of MEC transmission links in highly dynamic environments. This architecture facilitates the coordinated optimization between MEC resources and SAGIN nodes, effectively supporting seamless communication and computing services for mobile users. This design enables MEC applications in the SAGIN environment to more efficiently adapt to network condition fluctuations, enhance the uplink channel conditions, and improve computation offloading efficiency, thereby minimizing overall system latency to the greatest extent and delivering enhanced quality of service (QoS).

In this paper, we propose a task offloading and wireless resource management strategy for the FA-assisted MEC-SAGIN system. To minimize the total computation delay (TCD) and enhance the QoS for edge computing users, we jointly optimize the FA port positions, UAV location, and resource allocation. This study not only demonstrates the potential of FA in handling MEC tasks within SAGIN systems but also offers a novel solution for communication networks in complex environments.

B. Contributions and Organization

The main contributions of this paper are summarized as follows:

- We propose a novel FA-assisted MEC-SAGIN system, which helps ease the computational load at the GUs and the SU, and offers stable offloading in dynamic environments. By deploying FAs, the MEC-SAGIN system can better provide flexible adjustment capabilities in case of edge computing network congestion or device failures, thus enhancing the stability and reliability of the networks.
- To investigate MEC task offloading in an FA-assisted SAGIN system, we formulate a joint optimization problem involving task offloading strategies, computational resource allocation, FA port positions, UAV location, and the receive beamforming matrix.
- To address this highly non-convex and strongly coupled optimization problem, we employ the block coordinate descent (BCD) technique to decompose the original problem into four subproblems. In the joint task offloading and CPU allocation subproblem, we first derive a closed-form solution for the task offloading variable, while the CPU allocation is solved by introducing auxiliary variables and applying successive convex approximation (SCA). In addition, the UAV location optimization subproblem is also tackled using the SCA method. The receive beamforming subproblem is addressed via semidefinite relaxation (SDR) combined with Gaussian randomization, and the FA port selection subproblem is handled through a novel projected gradient descent (PGD)-based approach to cope with integer constraints.
- Simulation results demonstrate that the FA-assisted MEC-SAGIN system based on the proposed BCD algorithm achieves superior TCD performance compared with conventional fixed-position antenna (FPA) and random-port antenna schemes.

The structure of this paper is as follows: In Section II, we establish the system model and formulate the TCD minimization problem. The solution to this problem is provided in Section III. The simulation results are shown and discussed in Section IV. Finally, our conclusions are provided in Section V.

II. System Model

As shown in Fig. 1, we consider a SAGIN system oriented towards MEC tasks, comprising a satellite, a UAV, and K GUs. The MEC tasks include computation tasks from GUs with insufficient computing capabilities and service tasks from the satellite user (SU). Specifically, the satellite continuously senses and collects data while moving along a fixed trajectory, transmitting the data to the UAV for computation and processing. Each GU and SU has a task to execute, which can be partially offloaded to the UAV and partially computed locally. The UAV is equipped with an MEC server and N fixed-position antennas, serving as an MEC node. In addition, we assume that each GU and SU is equipped with an FA consisting of M ports, each of which can be activated if selected. The set of all GUs is denoted by $\mathcal{K} = \{1, 2, \cdots, K\}$, and the set of all FA ports at each GU or SU is denoted by $\mathcal{M} = \{1, 2, \cdots, M\}$. When transmitting signals, one port is selected for signal transmission. Specifically, the index of the

selected port can be represented by a variable $r_m \in \mathbb{Z}^{1\times 1}$, where $r_m \in \mathcal{M}$.

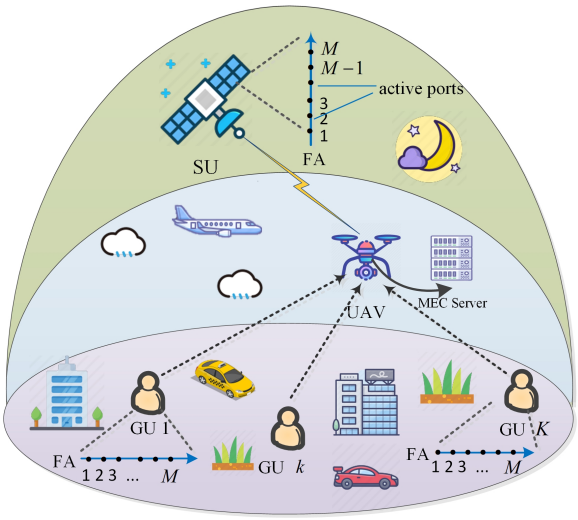

Fig. 1. Illustration of the FA-assisted MEC-SAGIN system, where K GUs and one SU offload their tasks to the edge computing node UAV via M-port FA.

A. Signal transmission

The channel vector between each GU, SU, and UAV is determined by the propagation environment and the position of the UAV. It is assumed that the far-field condition is satisfied between the GUs and the UAV, as well as between the SU and the UAV.

We consider the transmission link from the GUs and the SU to the UAV. In the ground network, the coordinates of the k-th GU can be denoted by $\mathbf{v}_k = (x_k, y_k)^{\mathrm{T}}$ since the height of each GU is approximated to be zero compared to the heights of UAV and satellite. In the air network, we define the coordinates of the UAV as

$$\mathbf{q} = (x, y)^{\mathrm{T}}, \tag{1}$$

and the height of the UAV is denoted as H_{U}. Therefore, the distance between the UAV and the k-th GU can be calculated as

$$q_k = \sqrt{\|\mathbf{q} - \mathbf{v}_k\|^2 + H_{\mathrm{U}}^2}. \tag{2}$$

Furthermore, the channel gain between the UAV and the k-th GU can be expressed as

$$h_k = \frac{\beta_0}{q_k^2}, \tag{3}$$

where β_0 is the path loss of the GU-to-UAV link at the reference distance of 1 m. In the space network, we denote the distance between the satellite and the UAV by d_o. Since the altitude of the satellite is very high, the positional change of the UAV has little effect on d_o. For simplification, we disregard the impact of the positional changes of the UAV on the distance between the satellite and the UAV. We model the SU-to-UAV wireless channel coefficient as

$$h_o = \delta_o(\frac{\lambda_o}{4\pi d_o})^2, \tag{4}$$

where δ_o is the beam gain, and λ_o denotes the wavelength of the SU-to-UAV transmission wave. The signal received at the UAV is formulated as follows

$$\mathbf{y} = \sum_{k=1}^{K} \sqrt{p_k h_k}\mathbf{g}_k(r_m^k)s_k + \sqrt{p_o h_o}\mathbf{g}_o(r_m^o)s_o + \mathbf{n}, \tag{5}$$

where $s_k \in \mathbb{C}^{1\times 1}$ and $s_o \in \mathbb{C}^{1\times 1}$ denote the data stream variables from the k-th GU and the SU, respectively, satisfying the distribution of zero mean and unit variance, p_k and p_o denote the transmit power of the k-th GU and the SU, respectively, and $\mathbf{n} \sim \mathcal{CN}(\mathbf{0}, \sigma^2\mathbf{I}_N)$ denotes the additive white Gaussian noise (AWGN). In addition, let $\mathbf{g}_k$, $\mathbf{g}_o$ denote the multiple-access channel vectors from the k-th GU and the SU to the UAV, respectively. A detailed description of the channel models for $\mathbf{g}_k$ and $\mathbf{g}_o$ will be provided in the next subsection.

It is assumed that the linear equalizer vectors $\mathbf{w}_k \in \mathbb{C}^{N\times 1}, \forall k \in \mathcal{K}$ and $\mathbf{w}_o \in \mathbb{C}^{N\times 1}$ are used to equalize the received signal of GUs and SU at the UAV, respectively. Thus, the received signal of the k-th GU and SU recovered at the UAV is respectively given by

$$\hat{s}_k = \mathbf{w}_k^{\mathrm{H}}\mathbf{y}, \tag{6}$$

$$\hat{s}_o = \mathbf{w}_o^{\mathrm{H}}\mathbf{y}. \tag{7}$$

In addition, we employ orthogonal-frequency-division multiple access (OFDMA) for the GU-to-UAV communication, with the k-th GU utilizing the frequency band B_k. Then the achievable transmission rate of the k-th GU at the UAV is given by

$$R_k = B_k\log_2(1 + \frac{p_k h_k|\mathbf{w}_k^{\mathrm{H}}\mathbf{g}_k(r_m^k)|^2}{\sigma^2 B_k|\mathbf{w}_k^{\mathrm{H}}|^2}). \tag{8}$$

The achievable transmission rate of the SU at the UAV is given by

$$R_o = B_o\log_2(1 + \frac{p_o h_o|\mathbf{w}_o^{\mathrm{H}}\mathbf{g}_o(r_m^o)|^2}{\sigma^2 B_o|\mathbf{w}_o^{\mathrm{H}}|^2}), \tag{9}$$

where B_o represents the channel bandwidth of the SU. For tractability and fairness, we assume equal bandwidth allocation for all users.

B. Channel Model

In this subsection, we present a detailed explanation of the multiple-access channel vectors $\mathbf{g}_k$ and $\mathbf{g}_o$. For simplicity, the numbers of transmit and receive paths are denoted by L_t and L_r, respectively.

1) Channel vector of the k-th GU-to-UAV transmission link $\mathbf{g}_k$: We first provide the expression of $\mathbf{g}_k$, which is given by

$$\mathbf{g}_k(r_m^k) = \mathbf{A}_k^{\mathrm{H}}\mathbf{O}_k\mathbf{u}_k(r_m^k), \tag{10}$$

where

$$\mathbf{A}_k = [\mathbf{a}_k(1), \mathbf{a}_k(2), \cdots, \mathbf{a}_k(N)] \in \mathbb{C}^{L_r\times N} \tag{11}$$

represents the field response vectors of all the N receive antennas at the UAV and $\mathbf{u}_k$ represents the coefficients of multi-path responses from the k-th GU to the reference point in the receive region. In addition, we define the path response matrix from the transmit FA port of the k-th GU to the fixed-position antenna of UAV as $\mathbf{O}_k \in \mathbb{C}^{L_r\times L_t}$.

To further clarify the expressions of $\mathbf{a}_k(n)$ and $\mathbf{u}_k(r_m^k)$, we next specify the angles involved in the transmission process and the distances between adjacent antennas and ports. Fig. 2 depicts the coordinates for the transmit and receive regions in an FA-assisted MEC-SAGIN system. The physical elevation and azimuth departure angles (AoDs) of the α-th $(0 \le \alpha \le L_t)$ transmit path from the selected port of the FA at the k-th GU to the scatterers are denoted by $\theta_{k,t}^{\alpha} \in [-\frac{\pi}{2}, \frac{\pi}{2}]$ and $\phi_{k,t}^{\alpha} \in [0, 2\pi]$, respectively. In addition, the elevation and azimuth arrival angles (AoAs) of the γ-th $(0 \le \gamma \le L_r)$ receive path from the scatterer to the received antenna at the UAV are denoted by $\theta_{k,r}^{\gamma} \in [-\frac{\pi}{2}, \frac{\pi}{2}]$ and $\phi_{k,r}^{\gamma} \in [0, 2\pi]$, respectively. For convenience, we define the coordinates of the m-th transmit FA port at the k-th GU as

$$d_{r_m^k} = \frac{2(r_m^k - 1) - M + 1}{2} d_{\mathrm{FA}}, \tag{12}$$

and the coordinates of the n-th receive antenna at the UAV as

$$d_{\mathrm{U}_n} = \frac{2(n-1) - N + 1}{2} d_{\mathrm{UAV}}, \tag{13}$$

where d_{FA} and d_{UAV} respectively represent the spacing between adjacent ports and adjacent fixed-position antennas.

Next, we derive the path difference in the transmission from GUs to the UAV, based on which the transmit field response vector $\mathbf{u}_k(r_m^k)$ and the receive field response vector $\mathbf{a}_k(n)$ are formulated. Along the k-th GU-to-UAV transmission link, let $l_{k,t}^{\alpha}$ and $l_{k,r}^{\gamma}$ denote the distances from the scatterer to the origin on the α-th transmit path and the γ-th receive path, respectively. The propagation path difference between the position of the m-th selected FA port and the origin is expressed as [40]

$$\rho_{k,\alpha}(r_m^k) = -d_{r_m^k} \sin\theta_{k,t}^{\alpha} - \frac{d_{r_m^k}^2 \sin^2\theta_{k,t}^{\alpha}}{2 l_{k,t}^{\alpha}}. \tag{14}$$

Then, the propagation path difference between the position of the n-th fixed-position antenna at the UAV and the origin is given by [40]

$$\rho_{k,\gamma}(n) = -d_{\mathrm{U}_n} \sin\theta_{k,r}^{\gamma} - \frac{d_{\mathrm{U}_n}^2 \sin^2\theta_{k,r}^{\gamma}}{2 l_{k,r}^{\gamma}}. \tag{15}$$

Herein, $\mathbf{a}_k(n)$ can be written as

$$\mathbf{a}_k(n) = [e^{j\frac{2\pi}{\lambda}\rho_{k,1}(n)}, e^{j\frac{2\pi}{\lambda}\rho_{k,2}(n)}, \ldots, e^{j\frac{2\pi}{\lambda}\rho_{k,L_r}(n)}]^{\mathrm{T}} \in \mathbb{C}^{L_r \times 1}, \tag{16}$$

and the field-response vector of the m-th FA at the k-th GU is given by

$$\mathbf{u}_k(r_m^k) = [e^{j\frac{2\pi}{\lambda}\rho_{k,1}(r_m^k)}, e^{j\frac{2\pi}{\lambda}\rho_{k,2}(r_m^k)}, \ldots, e^{j\frac{2\pi}{\lambda}\rho_{k,L_t}(r_m^k)}]^{\mathrm{T}} \in \mathbb{C}^{L_t \times 1}.$$

2) Channel vector of SU-to-UAV transmission link $\mathbf{g}_o$ *:* Now we introduce the expression for $\mathbf{g}_o \in \mathbb{C}^{N \times 1}$, the multiple-access channel vector from the SU to the UAV, given by

$$\mathbf{g}_o(r_m^o) = \mathbf{A}_o^{\mathrm{H}} \mathbf{O} \mathbf{u}_o(r_m^o), \tag{17}$$

where

$$\mathbf{A}_o = [\mathbf{a}_o(1), \mathbf{a}_o(2), \cdots, \mathbf{a}_o(N)] \in \mathbb{C}^{L_r \times N} \tag{18}$$

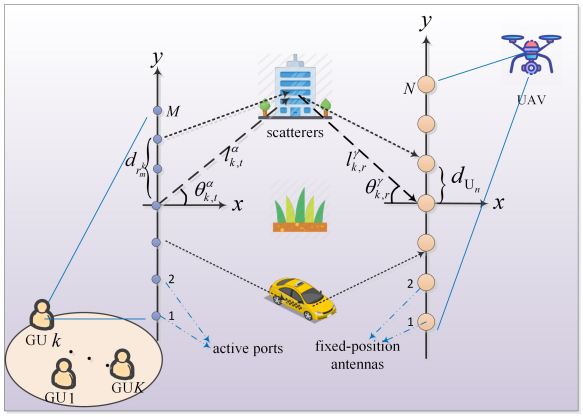

Fig. 2. Illustration of the coordinates for transmit and receive regions in FA-assisted MEC-SAGIN system.

represents the receive field response vectors of all the N antennas at the UAV, $\mathbf{u}_o$ represents the coefficients of multi-path responses from the SU to the reference point in the receive region, and $\mathbf{O} \in \mathbb{C}^{L_r \times L_t}$ represents the path response matrix from the SU to the UAV. Along the SU-to-UAV transmission link, let $l_{o,t}^{\alpha}$ and $l_{o,r}^{\gamma}$ denote the distances from the scatterer to the origin on the α-th transmit path and the γ-th receive path, respectively. Similarly, the propagation path differences between the position of the m-th selected FA port of the SU and the origin, and between the position of the n-th fixed-position antenna at the UAV and the origin, are denoted as

$$\rho_{o,\alpha}(r_m^o) = -d_{r_m^o} \sin\theta_{o,t}^{\alpha} - \frac{d_{r_m^o}^2 \sin^2\theta_{o,t}^{\alpha}}{2 l_{o,t}^{\alpha}} \tag{19}$$

and

$$\rho_{o,\gamma}(n) = -d_{\mathrm{U}_n} \sin\theta_{o,r}^{\gamma} - \frac{d_{\mathrm{U}_n}^2 \sin^2\theta_{o,r}^{\gamma}}{2 l_{o,r}^{\gamma}}, \tag{20}$$

respectively [40]. Therefore, $\mathbf{a}_o(n)$ can be written as

$$\mathbf{a}_o(n) = [e^{j\frac{2\pi}{\lambda}\rho_{o,1}(n)}, e^{j\frac{2\pi}{\lambda}\rho_{o,2}(n)}, \ldots, e^{j\frac{2\pi}{\lambda}\rho_{o,L_r}(n)}]^{\mathrm{T}} \in \mathbb{C}^{L_r \times 1}, \tag{21}$$

and the field response matrix corresponding to the activated port r_m^o of the SU is given by

$$\mathbf{u}_o(r_m^o) = [e^{j\frac{2\pi}{\lambda}\rho_{o,1}(r_m^o)}, e^{j\frac{2\pi}{\lambda}\rho_{o,2}(r_m^o)}, \ldots, e^{j\frac{2\pi}{\lambda}\rho_{o,L_t}(r_m^o)}]^{\mathrm{T}} \in \mathbb{C}^{L_t \times 1}.$$

C. Task Computing

In this subsection, we introduce the computing models of the system, including the local computing model and the edge computing model. Let l_k, l_o, C, D_o and D_k denote the offloading ratio of the task for the k-th GU, the offloading ratio of the task for the SU, the required CPU cycles for computing one bit of the tasks, the total computational task size of the SU, and the total computational task size of the k-th GU, respectively. It is assumed that the task-input bits are bit-wise independent. Each GU and SU can perform part of its own computation task locally and upload the rest of the task to the UAV for calculation.

1) Local computing: For local computing, the k-th GU calculates the total tasks of $(1-l_k)D_k$ bits. Denoting the local CPU frequency of the k-th GU as $f_{k,\mathrm{loc}}$ cycles per second, the time required for local computing is formulated as

$$t_{k,\mathrm{loc}} = \frac{(1-l_k)D_k C}{f_{k,\mathrm{loc}}}. \tag{22}$$

Moreover, SU calculates the total tasks of $(1-l_o)D_o$ bits. Denoting the local CPU frequency of the SU as $f_{o,\mathrm{loc}}$ cycles per second, the time required for local computing is formulated as

$$t_{o,\mathrm{loc}} = \frac{(1-l_o)D_o C}{f_{o,\mathrm{loc}}}. \tag{23}$$

2) Edge computing: The offloading time delay of the k-th GU and SU to the UAV can be respectively expressed as

$$t_{k,\mathrm{up}} = \frac{l_k D_k}{R_k}, \tag{24}$$

$$t_{o,\mathrm{up}} = \frac{l_o D_o}{R_o} + T_o, \tag{25}$$

where T_o is the one-way propagation delay between the satellite and the UAV. The time delay for computing the task of the k-th GU and SU at the UAV is given by

$$t_{k,\mathrm{com}} = \frac{l_k D_k C}{f_k}, \tag{26}$$

$$t_{o,\mathrm{com}} = \frac{l_o D_o C}{f_o}, \tag{27}$$

where f_k and f_o represent the computation capability allocated by the UAV to the k-th GU and SU, respectively. Since the data size of the computation results is much smaller than that of the offloaded computing data, the downlink transmission latency is negligible.

D. Problem Formulation

In this work, we aim to minimize the maximum TCD of the proposed FA-assisted MEC-SAGIN system by jointly optimizing the UAV location $\mathbf{q} = (x, y)^{\mathrm{T}}$, the offloading ratio $\mathbf{l} = \{l_o, \{l_k\}_{k\in\mathcal{K}}\}$, the computing frequency assignment $\mathbf{f} = \{f_o, \{f_k\}_{k\in\mathcal{K}}\}$, the beamforming matrix $\mathbf{W} = \{\mathbf{w}_o, \{\mathbf{w}_k\}_{k\in\mathcal{K}}\}$, and the FA port selection variable $\mathbf{r} = \{r_m^o, \{r_m^k\}_{k\in\mathcal{K}}\}$. The corresponding optimization problem is formulated as [1]

$$\min_{\mathbf{q},\mathbf{l},\mathbf{f},\mathbf{W},\mathbf{r},T} \quad T \tag{28a}$$

$$\text{s.t.} \quad T \geq \max\{t_{o,\mathrm{loc}}, t_{o,\mathrm{up}} + t_{o,\mathrm{com}}\}, \tag{28b}$$

$$T \geq \max\{t_{k,\mathrm{loc}}, t_{k,\mathrm{up}} + t_{k,\mathrm{com}}\}, \quad \forall k, \tag{28c}$$

$$\|\mathbf{w}_o\|^2 + \sum_{k=1}^{K} \|\mathbf{w}_k\|^2 \leq P_{\max}, \tag{28d}$$

$$0 \leq l_o \leq 1, \tag{28e}$$

$$0 \leq l_k \leq 1, \quad \forall k, \tag{28f}$$

$$0 \leq f_o \leq f_{\mathrm{total}}, \tag{28g}$$

$$0 \leq f_k \leq f_{\mathrm{total}}, \quad \forall k, \tag{28h}$$

$$\sum_{k=1}^{K} f_k + f_o \leq f_{\mathrm{total}}, \tag{28i}$$

$$r_m^k \in \mathcal{M}, \quad \forall k, \tag{28j}$$

$$r_m^o \in \mathcal{M}, \tag{28k}$$

where $P_{\max}$ and f_{total} represent the maximum transmission power constraint and the maximum number of CPU cycles for the UAV, respectively.

III. Algorithm Design

Problem (28) is inherently non-convex, and the optimization variables are intricately coupled, which poses significant challenges for direct solution. To address this, we employ the BCD method. This technique transforms the problem into a more tractable form by decoupling the five optimization variables, allowing for an iterative solution. Specifically, we first update the UAV location $\mathbf{q}$ given the offloading ratio $\mathbf{l}$, computing frequency assignment $\mathbf{f}$, the equalizer matrix $\mathbf{W}$, and the FA port selection $\mathbf{r}$. Second, we update the offloading ratio $\mathbf{l}$ and computing frequency assignment $\mathbf{f}$ given $\mathbf{W}$, $\mathbf{q}$, and $\mathbf{r}$. Then we optimize the receiver beamforming $\mathbf{W}$ given $\mathbf{l}$, $\mathbf{f}$, $\mathbf{q}$ and $\mathbf{r}$. Finally, the FA ports $\mathbf{r}$ are updated given $\mathbf{W}$, $\mathbf{l}$, $\mathbf{f}$ and $\mathbf{q}$. Repeat the above process until convergence.

A. UAV Location Optimization

Given the variables $\mathbf{l}$, $\mathbf{W}$, $\mathbf{r}$, and $\mathbf{f}$, Problem (28) for UAV location design can be simplified to

$$\min_{\mathbf{q},T} \quad T \tag{29a}$$

$$\text{s.t.} \quad T \geq \max\{t_{o,\mathrm{loc}}, t_{o,\mathrm{up}} + t_{o,\mathrm{com}}, t_{k,\mathrm{loc}}\} \quad \forall k, \tag{29b}$$

$$T \geq \frac{l_k D_k}{R_k} + \frac{l_k D_k C}{f_k}, \quad \forall k. \tag{29c}$$

[1]To evaluate the lower bound on the total delay achievable by deploying FAs in the MEC-SAGIN system, we assume ideal FA port switching with zero switching delay in the theoretical analysis. Taking into account that each FA reconfiguration in a practical system incurs a nonzero delay, we further assume that the additional latency caused by FA switching can be upper-bounded as $\Delta T_{\mathrm{FA}} \leq N_{\mathrm{sw}} \tau_{\mathrm{switch}}$, where N_{sw} denotes the number of switching operations. Within the range of parameters under consideration, the corresponding switching delay of this item is several orders of magnitude smaller than the communication and computing delays. Therefore, ignoring these switching terms does not affect the main conclusions of this work, while a more detailed hardware-aware modeling of switching losses will be pursued in our future investigation of robust FA system design.

Then we can transform the constraint (29c) as follows

$$R_k \geq \frac{l_k D_k}{T - \frac{l_k D_k C}{f_k}}, \quad \forall k. \tag{30}$$

Note that Problem (29) is non-convex due to the non-convexity of the logarithm terms in R_k. To resolve this issue, the denominator of R_k can be efficiently transformed using the SCA method. R_k can be expressed in a convex form with respect to $\|\mathbf{q}-\mathbf{v}_k\|^2$, since the function $\log(1+a/(b+x))$ is convex in x for positive constants a and b. According to the properties of convex functions, the first-order Taylor expansion at any point provides a global lower bound, which ensures that the approximated problem remains tractable while maintaining solution quality. Then, let $\mathbf{q}^{(j)} = \{x^{(j)}, y^{(j)}\}^{\mathrm{T}}$ denote the UAV location in the j-th iteration. We derive the lower bound of R_k as follows

$$\begin{aligned} R_k &= B_k \log_2(1 + \frac{p_k h_k |\mathbf{w}_k^{\mathrm{H}} \mathbf{g}_k|^2}{\sigma^2 B_k |\mathbf{w}_k^{\mathrm{H}}|^2}) \\ &= B_k \log_2(1 + \frac{p_k \beta_0 |\mathbf{w}_k^{\mathrm{H}} \mathbf{g}_k|^2}{\sigma^2 B_k |\mathbf{w}_k^{\mathrm{H}}|^2 (\|\mathbf{q}-\mathbf{v}_k\|^2 + H_{\mathrm{U}}^2)}) \\ &\geq B_k \log_2(1 + \frac{p_k \beta_0 |\mathbf{w}_k^{\mathrm{H}} \mathbf{g}_k|^2}{\sigma^2 B_k |\mathbf{w}_k^{\mathrm{H}}|^2 (\|\mathbf{q}^{(j)}-\mathbf{v}_k\|^2 + H_{\mathrm{U}}^2)}) \\ &+ B_k \frac{1}{\mathrm{In}2} (\frac{1}{1 + \frac{p_k \beta_0 |\mathbf{w}_k^{\mathrm{H}} \mathbf{g}_k|^2}{\sigma^2 B_k |\mathbf{w}_k^{\mathrm{H}}|^2 (\|\mathbf{q}^{(j)}-\mathbf{v}_k\|^2 + H_{\mathrm{U}}^2)}}) \\ &\times (-\frac{p_k \beta_0 |\mathbf{w}_k^{\mathrm{H}} \mathbf{g}_k|^2}{\sigma^2 B_k |\mathbf{w}_k^{\mathrm{H}}|^2}) \frac{\|\mathbf{q}-\mathbf{v}_k\|^2 - \|\mathbf{q}^{(j)}-\mathbf{v}_k\|^2}{(\|\mathbf{q}^{(j)}-\mathbf{v}_k\|^2 + H_{\mathrm{U}}^2)^2} \triangleq \hat{R}_k. \end{aligned} \tag{31}$$

Then, Problem (29) can be reformulated as

$$\begin{aligned} \min_{\mathbf{q}, T} \quad & T && (32a) \\ \text{s.t.} \quad & T \geq \max\{t_{o,\mathrm{loc}}, t_{o,\mathrm{up}} + t_{o,\mathrm{com}}, t_{k,\mathrm{loc}}\} \quad \forall k, && (32b) \\ & \hat{R}_k \geq \frac{l_k D_k}{T - \frac{l_k D_k C}{f_k}}, \quad \forall k, && (32c) \end{aligned}$$

which is convex and can thus be efficiently solved by utilizing convex optimization software.

B. Offloading Volume and Computing Frequency Optimization

For any given $\mathbf{q}, \mathbf{W}, \mathbf{r}$, the offloading volume of the users' tasks and the computing frequency assignment at the UAV of Problem (28) can be optimized by solving the following problem

$$\begin{aligned} \min_{\mathbf{l}, \mathbf{f}} \quad & T && (33) \\ \text{s.t.} \quad & (28\text{b}), (28\text{c}), (28\text{e}), (28\text{f}), (28\text{g}), (28\text{h}), (28\text{i}). \end{aligned}$$

Since Problem (33) remains intractable, we perform alternating optimization of $\mathbf{l}$ and $\mathbf{f}$, as detailed below.

1) Offloading Volume Optimization: Obviously, Problem (33) is a linear optimization problem with respect to $\mathbf{l}$, and therefore we have

$$\begin{aligned} T_i &= \max\{t_{i,\mathrm{loc}}, t_{i,\mathrm{up}} + t_{i,\mathrm{com}}\}, \quad i \in \mathcal{K} \cup \{o\}, && (34) \\ &= \begin{cases} \frac{(1-l_i) D_i C}{f_{i,\mathrm{loc}}}, & 0 \leq l_i \leq \frac{(D_i C - f_{i,\mathrm{loc}} T_i) R_i f_i}{D_i (C R_i f_i + f_i f_{i,\mathrm{loc}} + C R_i f_{i,\mathrm{loc}})}, \\ \frac{l_i D_i}{R_i} + T_i + \frac{l_i D_i C}{f_i}, & \frac{(D_i C - f_{i,\mathrm{loc}} T_i) R_i f_i}{D_i (C R_i f_i + f_i f_{i,\mathrm{loc}} + C R_i f_{i,\mathrm{loc}})} \leq l_i \leq 1, \end{cases} \end{aligned}$$

where $T_i = 0, \forall i \in \mathcal{K}$. Then, the offloading vector $\mathbf{l}^{\mathrm{opt}}$ is given by

$$l_i^{\mathrm{opt}} = \frac{(D_i C - f_{i,\mathrm{loc}} T_i) R_i f_i}{D_i (C R_i f_i + f_i f_{i,\mathrm{loc}} + C R_i f_{i,\mathrm{loc}})}, \forall i \in \mathcal{K} \cup \{o\}. \tag{35}$$

2) Computing Frequency Optimization: Given $\mathbf{q}, \mathbf{W}, \mathbf{r}$, and $\mathbf{l} = \mathbf{l}^{\mathrm{opt}}$, the subproblem of $\mathbf{f}$ can be rewritten as follows

$$\begin{aligned} \min_{\mathbf{f}} \quad & \max_{i \in \mathcal{K} \cup \{o\}} \{\frac{(D_i f_i + D_i C R_i + T_i R_i f_i) C}{C R_i f_i + f_i f_{i,\mathrm{loc}} + C R_i f_{i,\mathrm{loc}}}\} && (36) \\ \text{s.t.} \quad & (28\text{g}), (28\text{h}), (28\text{i}). \end{aligned}$$

It is observed that Problem (36) is non-convex. By introducing the auxiliary variable ξ, Problem (36) is formulated as

$$\begin{aligned} \min_{\mathbf{f}, \xi} \quad & \xi && (37a) \\ \text{s.t.} \quad & \xi \geq \frac{(D_i f_i + D_i C R_i + T_i R_i f_i) C}{C R_i f_i + f_i f_{i,\mathrm{loc}} + C R_i f_{i,\mathrm{loc}}}, i \in \mathcal{K} \cup \{o\}, && (37b) \\ & (28\text{g}), (28\text{h}), (28\text{i}). \end{aligned}$$

Considering that both the numerator and denominator in constraint (37b) contain f_i, we introduce auxiliary variables $\mathbf{e} = \{e_i, i \in \mathcal{K} \cup \{o\}\}$ and $\mathbf{m} = \{m_i, i \in \mathcal{K} \cup \{o\}\}$, then constraint (37b) can be reformulated as follows

$$\frac{C D_i + C T_i R_i}{e_i} \leq C R_i + f_{i,\mathrm{loc}} + \frac{C R_i f_{i,\mathrm{loc}}}{f_i}, \tag{38a}$$

$$\frac{C D_i C R_i}{m_i} \leq f_i (C R_i + f_{i,\mathrm{loc}}) + C R_i f_{i,\mathrm{loc}}, \tag{38b}$$

$$e_i + m_i \leq \xi. \tag{38c}$$

Since constraint (38a) remains non-convex, we use the SCA method to further transform the constraint into a convex form as follows

$$\begin{aligned} &\frac{C D_i + C T_i R_i}{e_i} \\ &\leq C R_i + f_{i,\mathrm{loc}} + \frac{C R_i f_{i,\mathrm{loc}}}{f_i^{(j)}} - \frac{C R_i f_{i,\mathrm{loc}}}{f_i^{(j),2}} (f_i - f_i^{(j)}), \end{aligned} \tag{39}$$

where $f_i^{(j)}$ represents the solution obtained from the previous iteration. Then, Problem (36) can be converted to a convex problem which is given by

$$\begin{aligned} \min_{\mathbf{f}, \mathbf{e}, \mathbf{m}, \xi} \quad & \xi && (40) \\ \text{s.t.} \quad & (28\text{g}), (28\text{h}), (28\text{i}), (38\text{b}), (38\text{c}), (39). \end{aligned}$$

Therefore, Problem (40) can be solved by standard convex solver packages, such as CVX. The procedure of solving Problem (33) is summarized in Algorithm 1.

Algorithm 1 Joint Optimization of $\mathbf{l}$ and $\mathbf{f}$ Given $\mathbf{r}$, $\mathbf{W}$ and $\mathbf{q}$.

1: Initialize the accuracy ϵ, the iteration index $j = 0$, the maximum number of iterations $j_{\max}$, set feasible $\mathbf{f}^{(0)}$.
2: Calculate $\mathbf{l}^{(j)}$ using (35).
3: With $\mathbf{l}^{(j)}$, calculate $\mathbf{f}^{(j)}$ by solving Problem (40).
4: If $j > j_{\max}$ or the objective function converges $|T^{(j+1)} - T^{(j)}|/|T^{(j+1)}| < \epsilon$, terminate and output $\mathbf{l}^{\mathrm{opt}}$ and $\mathbf{f}^{\mathrm{opt}}$. Otherwise, set $j \leftarrow j+1$ and go to step 2.

C. Receive Beamforming Optimization

Given the UAV location $\mathbf{q}$, the offloading ratio $\mathbf{l}$, the computing frequency assignment $\mathbf{f}$ and the FA port selection variable $\mathbf{r}$, Problem (28) can be transformed to

$$\begin{aligned} \min_{\mathbf{W},T} \quad & T \\ \text{s.t.} \quad & \text{(28b), (28c), (28d).} \end{aligned} \tag{41}$$

To tackle Problem (41), constraints (28b) and (28c) can be simplified to

$$T \geq \max\{t_{k,\mathrm{loc}}, t_{o,\mathrm{loc}}\} \tag{42}$$

$$T \geq \frac{l_i D_i}{R_i} + T_i + \frac{l_i D_i C}{f_i}, i \in \mathcal{K} \cup \{o\}, \tag{43}$$

where $T_i = 0, \forall i \in \mathcal{K}$. Constraint (43) can be further written as

$$R_i \geq \frac{l_i D_i}{T - T_i - \frac{l_i D_i C}{f_i}}. \tag{44}$$

To solve this non-convex problem, SDR method is applied. We define

$$\hat{\mathbf{W}}_i = \begin{bmatrix} \mathbf{w}_i \\ 1 \end{bmatrix} \begin{bmatrix} \mathbf{w}_i^{\mathrm{H}} & 1 \end{bmatrix} \in \mathbb{C}^{(N+1)\times(N+1)}, i \in \mathcal{K} \cup \{o\}. \tag{45}$$

The achievable transmission rate of the GUs and SU at the UAV is equivalently expressed as

$$\begin{aligned} R_i &= B_i \log_2(1 + \frac{p_i h_i |\mathbf{w}_i^{\mathrm{H}} \mathbf{g}_i|^2}{\sigma^2 B_i |\mathbf{w}_i^{\mathrm{H}}|^2}) \\ &= B_i \log_2(p_i h_i |\mathbf{w}_i^{\mathrm{H}} \mathbf{g}_i|^2 + \sigma^2 B_k |\mathbf{w}_i^{\mathrm{H}}|^2) - B_i \log_2(\sigma^2 B_i |\mathbf{w}_i^{\mathrm{H}}|^2) \\ &= B_i \log_2(\mathrm{tr}(\hat{\mathbf{H}}_i \hat{\mathbf{W}}_i)) - B_i \log_2(\mathrm{tr}(\tilde{\mathbf{H}}_i \hat{\mathbf{W}}_i)), \ i \in \mathcal{K} \cup \{o\}, \end{aligned}$$

where

$$\hat{\mathbf{H}}_i \triangleq \begin{bmatrix} p_i h_i \mathbf{g}_i \mathbf{g}_i^{\mathrm{H}} + \sigma^2 B_i & \mathbf{0}_{N\times 1} \\ \mathbf{0}_{1\times N} & 0_{1\times 1} \end{bmatrix} \in \mathbb{C}^{(N+1)\times(N+1)}, \tag{46}$$

and

$$\tilde{\mathbf{H}}_i \triangleq \begin{bmatrix} \sigma^2 B_i \mathbf{I}_N & \mathbf{0}_{N\times 1} \\ \mathbf{0}_{1\times N} & 0_{1\times 1} \end{bmatrix} \in \mathbb{C}^{(N+1)\times(N+1)}. \tag{47}$$

Then, constraint (44) can be transformed into

$$B_i \log_2(\mathrm{tr}(\hat{\mathbf{H}}_i \hat{\mathbf{W}}_i)) - B_i \log_2(\mathrm{tr}(\tilde{\mathbf{H}}_i \hat{\mathbf{W}}_i)) \geq \frac{l_i D_i}{T - T_i - \frac{l_i D_i C}{f_i}}. \tag{48}$$

Similarly, constraint (28d) is equivalent to

$$\mathrm{tr}(\hat{\mathbf{W}}_o) + \sum_{k=1}^{K} \mathrm{tr}(\hat{\mathbf{W}}_k) - (K+1) \leq P_{\max}. \tag{49}$$

To convexify $B_i \log_2(\mathrm{tr}(\tilde{\mathbf{H}}_i \hat{\mathbf{W}}_i))$, we apply the SCA approach to constraint (48). It can be rewritten as

$$\begin{aligned} & B_i \log_2(\mathrm{tr}(\hat{\mathbf{H}}_i \hat{\mathbf{W}}_i)) \\ & \geq \frac{l_i D_i}{T - T_i - \frac{l_i D_i C}{f_i}} + B_i \log_2(\mathrm{tr}(\tilde{\mathbf{H}}_i \hat{\mathbf{W}}_i^{(j)})) \\ & + B_i \frac{1}{\mathrm{In}2} \mathrm{tr}(\frac{\tilde{\mathbf{H}}_i}{\mathrm{tr}(\tilde{\mathbf{H}}_i \hat{\mathbf{W}}_i^{(j)})} (\hat{\mathbf{W}}_i - \hat{\mathbf{W}}_i^{(j)})). \end{aligned} \tag{50}$$

Therefore, Problem (41) can be recast as follows

$$\begin{aligned} \min_{\hat{\mathbf{W}},T} \quad & T && \text{(51a)} \\ \text{s.t.} \quad & \text{(42), (49), (50),} \\ & \hat{\mathbf{W}}_i[N+1, N+1] = 1, && \text{(51b)} \\ & \hat{\mathbf{W}}_i \succeq 0, \quad \mathrm{rank}(\hat{\mathbf{W}}_i) = 1. && \text{(51c)} \end{aligned}$$

By dropping the rank-one constraint, Problem (51) is a standard semidefinite programming problem which can be solved using CVX. Then, we can use Gaussian randomization method to recover the optimal rank-one solution.

We denote $\hat{\mathbf{W}}_i^1$ as the rank-one relaxed solution to Problem (51), Σ as a diagonal matrix including the eigenvalues of $\hat{\mathbf{W}}_i^1$, and $\hat{\mathbf{W}}_i^1 = \mathbf{U}\Sigma\mathbf{U}^{\mathrm{H}}$ as the eigenvalue decomposition of $\hat{\mathbf{W}}_i^1$, where the columns of $\mathbf{U}$ are eigenvectors of $\hat{\mathbf{W}}_i^1$. Specifically, we generate 10000 random candidate vectors, i.e., $\mathbf{w}_i^{(j)} = \frac{\mathbf{U}\Sigma^{1/2}\boldsymbol{\tau}^j}{[\mathbf{U}\Sigma^{1/2}\boldsymbol{\tau}^j]_{N+1}}, j = 1, 2, \cdots, 10000$ where $\boldsymbol{\tau}^j$ represents a unit vector and follows $\boldsymbol{\tau}^j \sim \mathcal{CN}(\mathbf{0}, \mathbf{I}_{N+1})$. Then $\hat{\mathbf{W}}_i^{\mathrm{opt}}$ satisfies all the constraints in Problem (51) and the objective function T is selected as the minimum solution. Then we have $\mathbf{w}_i^{\mathrm{opt}} = [\mathbf{w}_i^{(j),*}]_{1:N}$. To ensure the convergence of the algorithm, extensive Gaussian randomization can be performed.

D. FA Ports Optimization

In this part, we optimize the position of FAs at the users, i.e., $\mathbf{r}$, to minimize the total tasks computation delay subject to the positive integers constraints of the activated ports. Then, the optimization problem is formulated as follows

$$\begin{aligned} \min_{\mathbf{r},T} \quad & T && \text{(52a)} \\ \text{s.t.} \quad & T \geq \max\{t_{k,\mathrm{loc}}, t_{o,\mathrm{loc}}\}, \forall k && \text{(52b)} \\ & T \geq \frac{l_i D_i}{R_i} + T_i + \frac{l_i D_i C}{f_i}, i \in \mathcal{K} \cup \{o\}, && \text{(52c)} \\ & \text{(28j), (28k),} \end{aligned}$$

where

$$R_i = B_i \log_2(1 + \frac{p_i h_i |\mathbf{w}_i^{\mathrm{H}} \mathbf{g}_i(r_m^i)|^2}{\sigma^2 B_i |\mathbf{w}_i^{\mathrm{H}}|^2}), \quad i \in \mathcal{K} \cup \{o\}. \tag{53}$$

Due to the integer non-convexity of constraints (28j), (28k), and (52c), it is not feasible to solve this problem directly via standard convex optimization techniques. Referring to [41], gradient descent (GD) presumes a continuous, differentiable domain and is largely agnostic to curvature, so it is mainly suitable for smooth problems with simple constraints. In contrast, FA port selection is discrete and integer-constrained. A relax-and-round GD approach often produces infeasible or oscillatory iterates and offers no monotone-descent guarantee under the coupled SINR constraints. Thus, we adopt a PGD algorithm to solve the FA port selection subproblem. In each iteration, we first optimize a virtual continuous port index. We then use a projection step to map this index to the nearest feasible discrete port. This two-step approach enforces integer feasibility without exhaustive search, guaranteeing convergence to a locally optimal solution of Problem (52).

For tractability, constraint (52b) is treated as a constant upper bound on the feasible region and is therefore omitted during the PGD updates. We further relax the discrete design by allowing a continuum of virtual ports and enforce the fact that only M ports can be activated via the projection step.

Specifically, denoting $f(r_m^i) = \frac{l_i D_i}{R_i} + T_i + \frac{l_i D_i C}{f_i}, i \in \mathcal{K} \cup \{o\}$, the update rule of the PGD method for $\mathbf{r}$ is given by

$$r_m^{i,(j+1)} = r_m^{i,(j)} - \mu \nabla_{r_m^{i,(j)}} f(r_m^i), \quad i \in \mathcal{K} \cup \{o\}, \tag{54}$$

$$r_m^{i,(j+1)} = \mathcal{N}\{r_m^{i,(j+1)}, \mathcal{M}\}, \quad i \in \mathcal{K} \cup \{o\}, \tag{55}$$

where Eq. (54) represents the updated $r_m^{i,(j+1)}$ value in the $(j+1)$-th iteration of the GD method and Eq. (55) ensures that the FA port solution in each iteration always satisfies the integer constraint through the projection function $\mathcal{N}\{\cdot\}$. In addition, $\nabla_{r_m^{i,(j)}} f(r_m^i)$ and μ denote the gradient of $f(r_m^i)$ at $r_m^{i,(j)}$ and the step size for the GD method, respectively. Next, we carry out a detailed derivation for $\nabla_{r_m^{i,(j)}} f(r_m^i)$. Using the chain rule, $\nabla_{r_m^i} f(r_m^i)$ can be expressed as

$$\nabla_{r_m^i} f(r_m^i) = \frac{\partial f(r_m^i)}{\partial R_i} \cdot \frac{\partial R_i}{\partial r_m^i}, \quad i \in \mathcal{K} \cup \{o\}, \tag{56}$$

where

$$\frac{\partial f(r_m^i)}{\partial R_i} = -\frac{l_i D_i}{R_i^2}, \tag{57}$$

$$\frac{\partial R_i}{\partial r_m^i} = \frac{B_i}{\mathrm{In}2}\left(\frac{1}{1 + \frac{p_i h_i |\mathbf{w}_i^{\mathrm{H}} \mathbf{g}_i(r_m^i)|^2}{\sigma^2 B_i |\mathbf{w}_i^{\mathrm{H}}|^2}}\right) \frac{p_i h_i}{\sigma^2 B_i |\mathbf{w}_i^{\mathrm{H}}|^2} \frac{\partial |\mathbf{w}_i^{\mathrm{H}} \mathbf{g}_i(r_m^i)|^2}{\partial r_m^i}. \tag{58}$$

Based on (58), it is important to derive the closed-form expression of $\frac{\partial |\mathbf{w}_i^{\mathrm{H}} \mathbf{g}_i(r_m^i)|^2}{\partial r_m^i}, \quad i \in \mathcal{K} \cup \{o\}$. Then, we have

$$\begin{aligned} \frac{\partial |\mathbf{w}_i^{\mathrm{H}} \mathbf{g}_i(r_m^i)|^2}{\partial r_m^i} &= \frac{\partial \mathbf{w}_i^{\mathrm{H}}}{\partial r_m^i} \mathbf{g}_i(r_m^i) \mathbf{g}_i(r_m^i)^{\mathrm{H}} \mathbf{w}_i \\ &+ \mathbf{w}_i^{\mathrm{H}} \frac{\partial (\mathbf{g}_i(r_m^i) \mathbf{g}_i(r_m^i)^{\mathrm{H}})}{\partial r_m^i} \mathbf{w}_i + \mathbf{w}_i^{\mathrm{H}} \mathbf{g}_i(r_m^i) \mathbf{g}_i(r_m^i)^{\mathrm{H}} \frac{\partial \mathbf{w}_i}{\partial r_m^i} \\ &= \mathbf{w}_i^{\mathrm{H}} \frac{\partial (\mathbf{g}_i(r_m^i) \mathbf{g}_i(r_m^i)^{\mathrm{H}})}{\partial r_m^i} \mathbf{w}_i. \end{aligned} \tag{59}$$

Since the beamforming vector $\mathbf{w}_i$ is optimized in a separate subproblem given the FA port selection r_m^i, it can be treated as a constant during the gradient computation with respect to r_m^i, i.e., $\frac{\partial \mathbf{w}_i}{\partial r_m^i} = 0$. This simplifies the chain rule differentiation process and enables efficient gradient-based optimization. For simplicity, we denote $\mathbf{g}_i(r_m^i) \mathbf{g}_i(r_m^i)^{\mathrm{H}} \triangleq \mathbf{G}_i \in \mathbb{C}^{N \times N}$, where

$$\mathbf{G}_i = (\mathbf{A}_i^{\mathrm{H}} \mathbf{O}_i \mathbf{u}_i(r_m^i))(\mathbf{A}_i^{\mathrm{H}} \mathbf{O}_i \mathbf{u}_i(r_m^i))^{\mathrm{H}}. \tag{60}$$

Since $\mathbf{A}_i$ and $\mathbf{O}_i$ are independent of r_m^i, it is only necessary to differentiate $\mathbf{u}_i(r_m^i) \mathbf{u}_i(r_m^i)^{\mathrm{H}}$ with respect to r_m^i. Then, we can denote $\mathbf{u}_i(r_m^i) \mathbf{u}_i(r_m^i)^{\mathrm{H}} \triangleq \mathbf{U}_i$ and derive $\mathbf{U}_i$ as shown in (65) at the top of this page. Based on (65), the element in the x-th row and y-th column of $\mathbf{U}_i$ can be rewritten as

$$[\mathbf{U}_i]_{x,y} = e^{j \frac{2\pi}{\lambda} (\rho_{i,x}(r_m^i) - \rho_{i,y}(r_m^i))}. \tag{61}$$

Now we take the derivative of each element in $\mathbf{U}_i$ with respect to r_m^i as follows

$$\begin{aligned} \frac{\partial [\mathbf{U}_i]_{x,y}}{\partial r_m^i} &= \frac{\partial}{\partial r_m^i} e^{j \frac{2\pi}{\lambda} (\rho_{i,x}(r_m^i) - \rho_{i,y}(r_m^i))} \\ &= e^{j \frac{2\pi}{\lambda} (\rho_{i,x}(r_m^i) - \rho_{i,y}(r_m^i))} \cdot j \frac{2\pi}{\lambda} \frac{\partial}{\partial r_m^i} \left(\rho_{i,x}(r_m^i) - \rho_{i,y}(r_m^i)\right). \end{aligned} \tag{62}$$

Based on (14), we derive the result for $\frac{\partial \rho_{i,\alpha}(r_m^i)}{\partial r_m^i}$ as follows

$$\begin{aligned} \frac{\partial \rho_{i,\alpha}(r_m^i)}{\partial r_m^i} &= -\sin\theta_{i,t}^{\alpha} \cdot \frac{\partial d_{r_m^i}}{\partial r_m^i} - \frac{\sin^2 \theta_{i,t}^{\alpha}}{2 l_t^{\alpha}} \cdot \frac{\partial d_{r_m^i}^2}{\partial r_m^i}, \\ &= -\sin\theta_{i,t}^{\alpha} \cdot d_{\mathrm{FA}} - \frac{\sin^2 \theta_{i,t}^{\alpha}}{l_t^{\alpha}} d_{r_m^i} \cdot d_{\mathrm{FA}}. \end{aligned} \tag{63}$$

Thus, we have

$$\begin{aligned} &\frac{\partial}{\partial r_m^i} \left(\rho_{i,x}(r_m^i) - \rho_{i,y}(r_m^i)\right) \\ &= -d_{\mathrm{FA}}(\sin\theta_{i,t}^x - \sin\theta_{i,t}^y) - d_{\mathrm{FA}} \cdot d_{r_m^i}\left(\frac{\sin^2 \theta_{i,t}^x}{l_t^x} - \frac{\sin^2 \theta_{i,t}^y}{l_t^y}\right). \end{aligned} \tag{64}$$

Finally, by substituting (64) into (62), then substituting (62) into (59), the gradient $\frac{\partial |\mathbf{w}_i^{\mathrm{H}} \mathbf{g}_i(r_m^i)|^2}{\partial r_m^i}$ at r_m^i can be computed as in (67), shown at the top of this page. Therefore, $\nabla_{r_m^{i,(j)}} f(r_m^i)$ can be derived as (68).

E. Projection Function $\mathcal{N}\{\cdot\}$ and Feasible Step Size

The projection function primarily ensures that FA ports are selected only within respective feasible regions. Given the assumption of virtual selectable points in the GD method, the projection function can thus be defined according to the nearest distance criterion as follows

$$\mathcal{N}\{r_m^{i,(j+1)}, \mathcal{M}\} \triangleright r_m^{i,(j+1)} = \min(\max(\lfloor r_m^{i,(j+1)} \rceil, 1), M), \tag{69}$$

where $\lfloor x \rceil$ represents the rounding of x to the nearest integer. In addition, referring to [42], we use the backtracking line search (BLS) method to determine the step size for the PGD method, as detailed in Algorithm 2.

Algorithm 2 Feasible Step Size Selection in the PGD Method for Solving Problem (52).

1: Initialize the step $\mu > 0$ and the initial point $\mathbf{r}^{(0)}$ of the PGD method. Set the iteration index $j = 1$, $\varpi \in (0, 0.5)$ and $\varphi \in (0, 1)$.
2: Calculate $r_m^{i,(j+1)} = \mathcal{N}\{r_m^{i,(j)} - \mu \nabla_{r_m^{i,(j)}} f(r_m^i), \mathcal{M}\}, \quad i \in \mathcal{K} \cup \{o\}$.
3: If $f(r_m^{i,(j+1)}) > f(r_m^{i,(j)}) - \varpi \mu \|\nabla_{r_m^{i,(j)}} f(r_m^i)\|^2$, update $\mu \leftarrow \varphi \mu$. Otherwise, set $j \leftarrow j + 1$ and go to step 2.

F. Complexity and Convergence Analysis

The overall algorithm for solving Problem (28) is summarized in Algorithm 3.

$$\mathbf{u}_i(r_m^i)\mathbf{u}_i(r_m^i)^{\mathrm{H}} = \begin{bmatrix} e^{j\frac{2\pi}{\lambda}(\rho_{i,1}(r_m^i)-\rho_{i,1}(r_m^i))} & e^{j\frac{2\pi}{\lambda}(\rho_{i,1}(r_m^i)-\rho_{i,2}(r_m^i))} & \dots & e^{j\frac{2\pi}{\lambda}(\rho_{i,1}(r_m^i)-\rho_{i,L_t}(r_m^i))} \\ e^{j\frac{2\pi}{\lambda}(\rho_{i,2}(r_m^i)-\rho_{i,1}(r_m^i))} & e^{j\frac{2\pi}{\lambda}(\rho_{i,2}(r_m^i)-\rho_{i,2}(r_m^i))} & \dots & e^{j\frac{2\pi}{\lambda}(\rho_{i,2}(r_m^i)-\rho_{i,L_t}(r_m^i))} \\ \vdots & \vdots & \ddots & \vdots \\ e^{j\frac{2\pi}{\lambda}(\rho_{i,L_t}(r_m^i)-\rho_{i,1}(r_m^i))} & e^{j\frac{2\pi}{\lambda}(\rho_{i,L_t}(r_m^i)-\rho_{i,2}(r_m^i))} & \dots & e^{j\frac{2\pi}{\lambda}(\rho_{i,L_t}(r_m^i)-\rho_{i,L_t}(r_m^i))} \end{bmatrix}. \tag{65}$$

$$\frac{\partial[\mathbf{U}_i]_{x,y}}{\partial r_m^i} = e^{j\frac{2\pi}{\lambda}(\rho_{i,x}(r_m^i)-\rho_{i,y}(r_m^i))}\cdot j\frac{2\pi}{\lambda}(-d_{\mathrm{FA}}(\sin\theta_{i,t}^x-\sin\theta_{i,t}^y)-d_{\mathrm{FA}}\cdot d_{r_m^i}(\frac{\sin^2\theta_{i,t}^x}{l_{i,t}^x}-\frac{\sin^2\theta_{i,t}^y}{l_{i,t}^y})). \tag{66}$$

$$\frac{\partial|\mathbf{w}_i^{\mathrm{H}}\mathbf{g}_i(r_m^i)|^2}{\partial r_m^i} = \mathbf{w}_i^{\mathrm{H}}\mathbf{A}_i^{\mathrm{H}}\mathbf{O}_i \begin{bmatrix} \frac{\partial[\mathbf{U}_i]_{1,1}}{\partial r_m^i} & \frac{\partial[\mathbf{U}_i]_{1,2}}{\partial r_m^i} & \dots & \frac{\partial[\mathbf{U}_i]_{1,L_t}}{\partial r_m^i} \\ \frac{\partial[\mathbf{U}_i]_{2,1}}{\partial r_m^i} & \frac{\partial[\mathbf{U}_i]_{2,2}}{\partial r_m^i} & \dots & \frac{\partial[\mathbf{U}_i]_{2,L_t}}{\partial r_m^i} \\ \vdots & \vdots & \ddots & \vdots \\ \frac{\partial[\mathbf{U}_i]_{L_t,1}}{\partial r_m^i} & \frac{\partial[\mathbf{U}_i]_{L_t,2}}{\partial r_m^i} & \dots & \frac{\partial[\mathbf{U}_i]_{L_t,L_t}}{\partial r_m^i}. \end{bmatrix}_{L_t\times L_t} \mathbf{O}_i^{\mathrm{H}}\mathbf{A}_i\mathbf{w}_i, \quad i\in\mathcal{K}\cup\{o\}. \tag{67}$$

$$\nabla_{r_m^{i,(j)}} f(r_m^i) =$$

$$-\frac{l_i D_i}{R_i^2}\cdot\frac{B_i}{\mathrm{In}2}\Big(\frac{1}{1+\frac{p_i h_i|\mathbf{w}_i^{\mathrm{H}}\mathbf{g}_i(r_m^i)|^2}{\sigma^2 B_i|\mathbf{w}_i^{\mathrm{H}}|^2}}\Big)\frac{p_i h_i}{\sigma^2 B_i|\mathbf{w}_i^{\mathrm{H}}|^2}\left[\mathbf{w}_i^{\mathrm{H}}\mathbf{A}_i^{\mathrm{H}}\mathbf{O}_i\begin{bmatrix} \frac{\partial[\mathbf{U}_i]_{1,1}}{\partial r_m^i} & \frac{\partial[\mathbf{U}_i]_{1,2}}{\partial r_m^i} & \dots & \frac{\partial[\mathbf{U}_i]_{1,L_t}}{\partial r_m^i} \\ \frac{\partial[\mathbf{U}_i]_{2,1}}{\partial r_m^i} & \frac{\partial[\mathbf{U}_i]_{2,2}}{\partial r_m^i} & \dots & \frac{\partial[\mathbf{U}_i]_{2,L_t}}{\partial r_m^i} \\ \vdots & \vdots & \ddots & \vdots \\ \frac{\partial[\mathbf{U}_i]_{L_t,1}}{\partial r_m^i} & \frac{\partial[\mathbf{U}_i]_{L_t,2}}{\partial r_m^i} & \dots & \frac{\partial[\mathbf{U}_i]_{L_t,L_t}}{\partial r_m^i}. \end{bmatrix}_{L_t\times L_t}\mathbf{O}_i^{\mathrm{H}}\mathbf{A}_i\mathbf{w}_i\right]_{r_m^i=r_m^{i,(j)}}, \tag{68}$$

Algorithm 3 Task Computation Delay Minimization Algorithm for the FA-Assisted MEC-SAGIN System

1: Initialization: Let $\mathbf{q}^{(0)} = \frac{1}{K}\sum_{k\in\mathcal{K}}\mathbf{v}_k$, $r_m^{i,(0)} = \arg\max_{m\in\mathcal{M}}|\,\widehat{\mathbf{w}}_i^{\mathrm{H}}\,\mathbf{g}_i(m)\,|^2$, $\mathbf{w}_i^{(0)} = \sqrt{\frac{P_{\max}}{K+1}}\frac{\mathbf{g}_i(r_m^{i,(0)})}{\|\mathbf{g}_i(r_m^{i,(0)})\|_2}$, $l_i^{(0)} = [\frac{(D_iC-f_{i,\mathrm{loc}}T_i)\,R_i^{(0)}\,f_i^{(0)}}{D_i(CR_i^{(0)}f_i^{(0)}+f_i^{(0)}f_{i,\mathrm{loc}}+CR_i^{(0)}f_{i,\mathrm{loc}})}]_0^1$, $f_i^{(0)} = f_{\mathrm{total}}/(K+1)$, and set the iteration index $k=1$.
2: With given $\mathbf{l}^{(k-1)},\mathbf{f}^{(k-1)},\mathbf{W}^{(k-1)},\mathbf{r}^{(k-1)}$, solve the UAV location subproblem and obtain $\mathbf{q}^{(k)}$.
3: With given $\mathbf{q}^{(k)},\mathbf{W}^{(k-1)},\mathbf{r}^{(k-1)}$, solve the joint offloading volume and computing frequency optimization subproblem and obtain $\mathbf{l}^{(k)}$ and $\mathbf{f}^{(k)}$.
4: With given $\mathbf{l}^{(k)},\mathbf{f}^{(k)},\mathbf{q}^{(k)},\mathbf{r}^{(k-1)}$, solve the receive beamforming subproblem and obtain $\mathbf{W}^{(k)}$.
5: With given $\mathbf{l}^{(k)},\mathbf{f}^{(k)},\mathbf{q}^{(k)},\mathbf{W}^{(k)}$, solve the FA port selection subproblem and obtain $\mathbf{r}^{(k)}$.
6: If the objective of Problem (28) converges, output $(\mathbf{q}^{(k)},\mathbf{l}^{(k)},\mathbf{f}^{(k)},\mathbf{W}^{(k)},\mathbf{r}^{(k)})$; otherwise set $k\leftarrow k+1$ and go to Step 2.

1) Complexity Analysis: We evaluate algorithmic complexity using the total count of floating-point operations, treating each addition or multiplication as one flop. The complexity is expressed with respect to the sizes of the matrices involved, and subsequently simplified by keeping only the dominant highest-order terms and omitting the remainder.

The proposed BCD algorithm jointly optimizes five variables with the following computational complexities. For UAV location optimization, the SCA method solves a convex problem with N_q iterations, yielding complexity $\mathcal{O}(N_q\cdot n_q^{3.5})$. The task offloading ratio optimization admits a closed-form solution given by Eq. (35), requiring only $\mathcal{O}(K+1)$ operations. For computational frequency allocation, the SCA-based approach requires N_f iterations to solve a convex problem with $3(K+1)+1$ variables, resulting in complexity $\mathcal{O}(N_f(K+1)^3)$. The receive beamforming optimization dominates the computational burden, where solving the SDP formulation with $(K+1)$ matrices of size $(N+1)\times(N+1)$ requires $\mathcal{O}(N_w((K+1)(N+1)^2)^{4.5})$, and subsequent Gaussian randomization with $N_{\mathrm{rand}}=10{,}000$ samples adds $\mathcal{O}(N_{\mathrm{rand}}(K+1)N^2)$, making the total beamforming complexity $\mathcal{O}(N_w(K+1)^{4.5}(N+1)^9)$. Finally, the FA port selection optimization employs PGD with backtracking line search, where each of N_{pgd} iterations involves gradient computation at complexity $\mathcal{O}((K+1)L_t^2N)$ and N_{bls} line search steps, yielding total complexity $\mathcal{O}(N_{\mathrm{pgd}}(N_{\mathrm{bls}}(K+1)+(K+1)L_t^2N))$. With N_{BCD} outer iterations, the overall algorithm complexity is $\mathcal{O}(N_{\mathrm{BCD}}\cdot\max\{N_q,N_f(K+1)^3,N_w(K+1)^{4.5}(N+1)^9,N_{\mathrm{pgd}}N_{\mathrm{bls}}(K+1)L_t^2N\})$.

2) Convergence Analysis: In this subsection, we analyze the convergence of Algorithm 3. We denote the TCD objective function as $F(\mathbf{q},\mathbf{l},\mathbf{f},\mathbf{W},\mathbf{r})$. In the k-th iteration, we have

$$\begin{aligned} &F\big(\mathbf{q}^{(k)},\mathbf{l}^{(k)},\mathbf{f}^{(k)},\mathbf{W}^{(k)},\mathbf{r}^{(k)}\big) \\ &\overset{(a)}{\geq} F\big(\mathbf{q}^{(k+1)},\mathbf{l}^{(k)},\mathbf{f}^{(k)},\mathbf{W}^{(k)},\mathbf{r}^{(k)}\big), \\ &\overset{(b)}{\geq} F\big(\mathbf{q}^{(k+1)},\mathbf{l}^{(k+1)},\mathbf{f}^{(k+1)},\mathbf{W}^{(k)},\mathbf{r}^{(k)}\big) \\ &\overset{(c)}{\geq} F\big(\mathbf{q}^{(k+1)},\mathbf{l}^{(k+1)},\mathbf{f}^{(k+1)},\mathbf{W}^{(k+1)},\mathbf{r}^{(k)}\big) \\ &\overset{(d)}{\geq} F\big(\mathbf{q}^{(k+1)},\mathbf{l}^{(k+1)},\mathbf{f}^{(k+1)},\mathbf{W}^{(k+1)},\mathbf{r}^{(k+1)}\big), \end{aligned}$$

where (a), (b) and (c) hold because (32), (35), (40) and (51) are the optimal solutions of the corresponding subproblems. (d) holds because the monotonic decrease and boundedness of the objective sequence $f(r_m^k)$, together with the Lipschitz continuity of the gradient, ensure that PGD with Armijo back-

tracking converges to a first-order stationary point. Moreover, with the bounded feasible set in Problem (28), the objective function has a finite lower bound. Hence, Problem (28) is guaranteed to converge.

G. Extended System Model with Multiple UAVs and Multiple SUs

To demonstrate scalability, we extend the system to U UAVs, O SUs, and K GUs. Let $\mathcal{U} = \{1, \ldots, U\}$, $\mathcal{O} = \{1, \ldots, O\}$, and $\mathcal{K} = \{1, \ldots, K\}$. Each user (GU/SU) employs an FA with M selectable ports $\mathcal{M} = \{1, \ldots, M\}$ and only one port is active per transmission. The u-th UAV is at $\mathbf{q}_u = (x_u, y_u)^{\mathrm{T}}$ with altitude H_{U}. Large-scale loss and multipath vectors follow the original definitions, now indexed by u. The distance between the UAV u and the k-th GU can be calculated as

$$q_{k,u} = \sqrt{\|\mathbf{q}_u - \mathbf{v}_k\|^2 + H_{\mathrm{U}}^2}, \qquad h_{k,u} = \beta_0 / q_{k,u}^2. \tag{70}$$

In addition, the user-to-UAV channel vectors can be rewritten as $\mathbf{g}_{k,u}(r_m^k)$ and $\mathbf{g}_{o,u}(r_m^o)$.

1) Signal transmission: At UAV u, the received signal is

$$\mathbf{y}_u = \sum_{k \in \mathcal{K} \cap \mathcal{S}_u} \sqrt{p_k h_{k,u}}\, \mathbf{g}_{k,u}(r_m^k)\, s_k + \sum_{o \in \mathcal{O} \cap \mathcal{S}_u} \sqrt{p_o h_{o,u}}\, \mathbf{g}_{o,u}(r_m^o)\, s_o + \mathbf{n}_u, \tag{71}$$

where $\mathbf{n}_u \sim \mathcal{CN}(\mathbf{0}, \sigma^2 \mathbf{I}_N)$ and $\mathcal{S}_u$ is the set served by UAV u. With OFDMA per UAV, the rate of user $i \in \mathcal{K} \cup \mathcal{O}$ at UAV u is

$$R_{i,u} = B_{i,u} \log_2\!\left(1 + \frac{p_i h_{i,u} \left|\mathbf{w}_{i,u}^{\mathrm{H}} \mathbf{g}_{i,u}(r_m^i)\right|^2}{\sigma^2 B_{i,u} \|\mathbf{w}_{i,u}\|^2}\right), \tag{72}$$

with linear equalizer $\mathbf{w}_{i,u} \in \mathbb{C}^{N \times 1}$ and per-UAV bandwidth budget as follows

$$\sum_{i \in \mathcal{K} \cup \mathcal{O}} B_{i,u} \le B_{\mathrm{total}}^{(u)}, \quad \forall u. \tag{73}$$

Moreover, for each user, only one FA port is active per transmission, i.e., $r_m^i \in \mathcal{M}$ and exactly one m is selected.

2) Task Computing: Let $a_{i,u} \in \{0, 1\}$ denote the association indicator, where each task is handled by exactly one UAV, i.e., $\sum_{u \in \mathcal{U}} a_{i,u} = 1$. With offloading ratio $l_i \in [0, 1]$, the edge computing time delays are given by

$$t_{i,\mathrm{up}} = \sum_u a_{i,u} \frac{l_i D_i}{R_{i,u}} + 1_{\, i \in \mathcal{O}} \sum_u a_{i,u} T_{i,u}, \tag{74}$$

$$t_{i,\mathrm{com}} = \sum_u a_{i,u} \frac{l_i D_i C}{f_{i,u}}, \tag{75}$$

and the per-UAV CPU constraint is

$$\sum_{i \in \mathcal{S}_u} f_{i,u} \le f_{\mathrm{total}}^{(u)}, \quad \forall u. \tag{76}$$

3) Problem Formulation: In this work, we aim to minimize the TCD of the proposed FA-assisted MEC-SAGIN system with multiple UAVs and SUs. The corresponding optimization problem is formulated as

$$\min_{\substack{\{\mathbf{q}_u\}, \{l_i\}, \{f_{i,u}\}, \\ \{\mathbf{w}_{i,u}\}, \{r_m^i\}, \{a_{i,u}\}, \\ \{B_{i,u}\}, T}} \quad T \tag{77a}$$

$$\text{s.t. } T \ge \max\{t_{i,\mathrm{loc}},\ t_{i,\mathrm{up}} + t_{i,\mathrm{com}}\}, \forall i, \tag{77b}$$

$$\sum_u a_{i,u} = 1, \ \ a_{i,u} \in \{0, 1\}, \ \forall i, \tag{77c}$$

$$0 \le l_i \le 1, \forall i, \tag{77d}$$

$$\sum_{i \in \mathcal{S}_u} f_{i,u} \le f_{\mathrm{total}}^{(u)}, \tag{77e}$$

$$\sum_{i \in \mathcal{S}_u} B_{i,u} \le B_{\mathrm{total}}^{(u)}, \ \forall u, \tag{77f}$$

$$B_{i,u} \ge 0, \ \ r_m^i \in \mathcal{M}, \ \forall i, u, \tag{77g}$$

$$\sum_{i \in \mathcal{S}_u} \|\mathbf{w}_{i,u}\|^2 \le P_{\max}^{(u)}. \tag{77h}$$

It is observed that the extended multi-UAV and SUs problem is non-convex due to the coupling among association, bandwidth, CPU allocation, FA-port selection, receiver design, and UAV locations. To address this, we adopt an alternating optimization framework that iteratively solves the following subproblems:

- Receiver Beamforming Optimization: Given $\{\mathbf{r}, \mathbf{l}, \mathbf{f}, \mathbf{B}, \mathbf{q}, \mathbf{A}\}$, Problem (77) is reduced to a receiver beamforming optimization subproblem. By using the SCA method, the $\mathbf{W}$ subproblem can be reduced into an SDR convex problem, which can be solved by CVX and then recovered by Gaussian randomization.
- UAV Location Optimization: Given $\{\mathbf{r}, \mathbf{l}, \mathbf{f}, \mathbf{B}, \mathbf{W}, \mathbf{A}\}$, Problem (77) is reduced to a UAV location subproblem. Due to the non-convexity of R_k, we can utilize the SCA method adopted in Problem (77) to rewrite R_k by its first-order Taylor expression, and solve the transformed convex problem iteratively to obtain the optimal UAV location.
- Offloading Volume and Computing Frequency Assignment Optimization: Given $\{\mathbf{r}, \mathbf{q}, \mathbf{B}, \mathbf{W}, \mathbf{A}\}$, the optimal CPU frequency $\mathbf{f}$ and offloading volume $\mathbf{l}$ can be jointly optimized by SCA method and then we can obtain the closed-form solutions for $\mathbf{l}$.
- Per-UAV Bandwidth Allocation Optimization: Given $\{\mathbf{r}, \mathbf{l}, \mathbf{f}, \mathbf{q}, \mathbf{W}, \mathbf{A}\}$, the per-UAV bandwidths are updated under individual bandwidth budgets via a first-order SCA that convexifies the non-convex rate expressions around the previous iterate, yielding a convex program solved efficiently.
- User-to-UAV Association Optimization: Given $\{\mathbf{r}, \mathbf{l}, \mathbf{f}, \mathbf{q}, \mathbf{W}, \mathbf{B}\}$, we first relax the $\mathbf{A}$-subproblem to a continuous formulation and then solve it using a greedy algorithm or the Hungarian method.

IV. Simulation results

In this section, we conduct experiments to evaluate the TCD performance of the FA-assisted MEC-SAGIN system

and validate the effectiveness of our proposed algorithms. We consider three GUs and an SU, where the GUs are uniformly distributed within a circular area centered at (50,0) with a radius of 50 meters. The main simulation parameters are listed in Table I. [2]

TABLE I
DEFAULT SIMULATION PARAMETER SETTINGS

Parameter	Value
Transmit power of users	$p_{\mathrm{k}} = p_{\mathrm{o}} = 1$ W
Average noise power	$\sigma^2 = -80$ dBm
Maximum number of CPU cycles at UAV	$f_{\mathrm{total}} = 2 \times 10^{10}$ cycles/s
Local CPU frequency of GUs and SU	$f_{k,\mathrm{loc}} = 5 \times 10^8$ cycles/s $f_{o,\mathrm{loc}} = 5 \times 10^8$ cycles/s
Propagation delay of SU	$T_o = 10$ ms
Total computational task size	$D_k = D_o = 3 \times 10^6$ bits
Required CPU cycles for computing one bit	$C = 2 \times 10^3$ cycles/bit
Channel bandwidth	$B_k = B_o = 10^6$ Hz
Number of channel paths	$L_r = L_t = 4$
Carrier wavelength	$\lambda = 5$ mm
Antenna spacing and port spacing	$d_{\mathrm{FA}} = d_{\mathrm{UAV}} = \lambda/2$
The AoDs and AoAs	$\theta^{\alpha}_{k,t} \in [-\frac{\pi}{2}, \frac{\pi}{2}]$ $\theta^{\gamma}_{k,r} \in [-\frac{\pi}{2}, \frac{\pi}{2}]$

The following subsection provides a detailed introduction to our simulation results. To clearly demonstrate the effectiveness of our proposed FA-assisted MEC-SAGIN design, we provide the following benchmark schemes:

- Conventional FPAs: Both the GUs and the SU are equipped with FPAs, with each user having M fixed-position antennas for signal transmission, spaced by $d_{\mathrm{FA}}(M-1)$.
- Random FAs: The activated ports of the FA at the GUs and SU are randomly selected, and other variables are optimized using the proposed algorithm.
- Proposed FAs (exhaustive method): The FA port selection variables of GUs and SU are optimized using the exhaustive search method, while the other variables are optimized using the proposed algorithm.
- Hybrid FAs: In this scheme, the users' antennas operate in the FPA mode for half of the transmission time and in the FA mode for the other half.
- Proposed FAs (penalty-based algorithm): The receive beamforming is optimized by the penalty algorithm and the other variables are optimized using our proposed algorithm.
- Fixed UAV location with FAs: The UAV is fixed at the initial position, while FA port selection and MEC resource allocation are optimized by our proposed algorithm.

Based on the six proposed schemes, we further evaluate the convergence performance of our proposed algorithm, the impact of the number of FA ports, and the TCD performance with respect to the total edge computing resource, user task size, number of edge computing users, number of channel paths, and FA port spacing.

[2]The simulation parameters in Table I are selected based on practical system specifications and validated against existing literature [5]-[7][16]-[18][23][26]-[29]. These parameter choices ensure the simulation reflects realistic deployment scenarios.

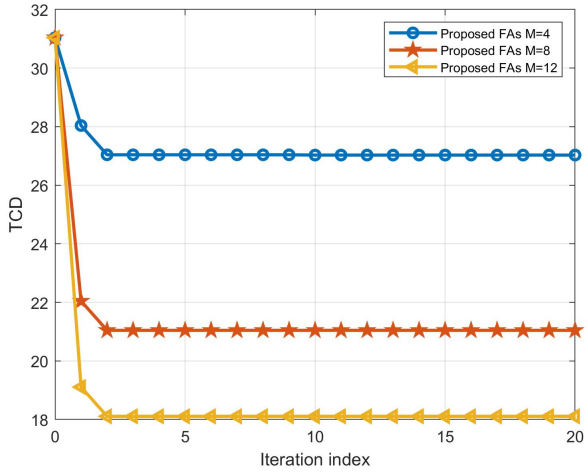

Fig. 3. Convergence of the proposed algorithm for different numbers of ports, $M = [4, 8, 12]$.

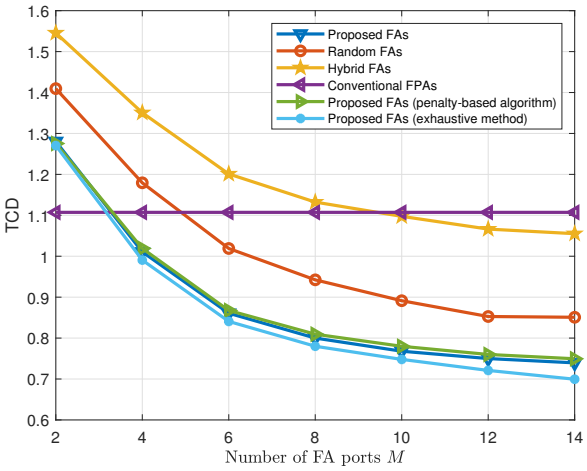

Fig. 4. TCD performance versus the number of FA ports M.

We first evaluate the convergence performance of the BCD algorithm under different numbers of FA ports in Fig. 3. It can be observed that the TCD decreases monotonically as the number of iterations increases. The proposed algorithm converges within five iterations, underscoring its effectiveness and low computational complexity.

Fig. 4 illustrates the impact of the number of FA ports on the TCD performance under different algorithms. Except for the conventional FPAs approach, the TCD of all FA-based algorithms exhibits a decreasing trend as M increases, owing to the enhanced degrees of freedom that contribute to reducing the overall completion time of edge computing tasks. However, as the number of antenna ports surpasses $M > 10$, the delay benefits from additional ports become marginal. This is because, with a fixed size of the FA, the TCD first decreases markedly as the number of ports M increases and then saturates. This phenomenon occurs because reducing the port spacing leads to stronger inter-port correlation. Increasing M initially introduces additional diversity that improves the

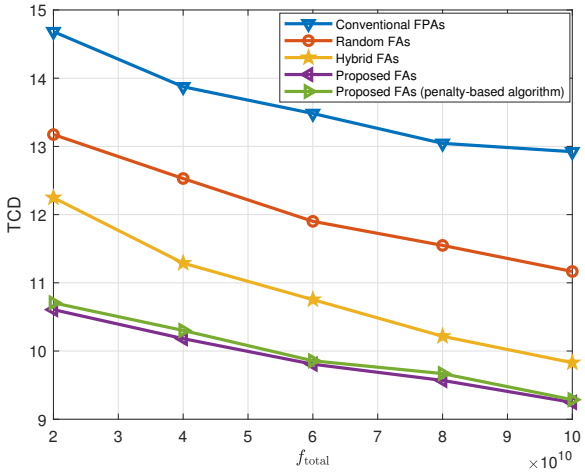

Fig. 5. TCD performance versus the edge computing resource f_{total} with different algorithms under $M = 10$.

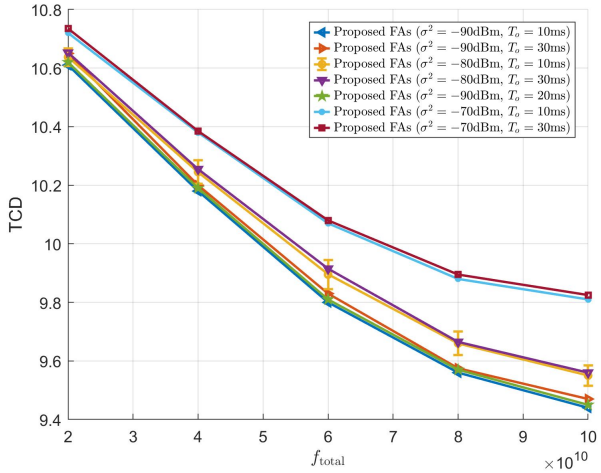

Fig. 6. TCD versus f_{total} under different noise power σ^2 and satellite–to-UAV propagation delay T_o.

uplink transmission rate and thereby reduces the total time delays. Therefore, as M grows, the enhanced correlation gradually diminishes the performance gain in computation time delay. Compared to the exhaustive search method, the BCD algorithm achieves near-optimal performance in the FA system, with an average degradation rate of only 7.14%. For small K, the penalty-based algorithm delivers nearly identical TCD to our proposed scheme. For a limited number of FA ports, the difference between conventional FPAs and FA-based schemes remains negligible. As the number of FA ports increases, FA-based schemes demonstrate a significant enhancement in the TCD performance compared to FPAs under equivalent conditions. In addition, both the Hybrid FAs and random FA schemes exhibit inferior TCD performance compared to the proposed BCD algorithm. The performance gap between the FAs scheme and the Hybrid FAs and random FAs schemes further expands as M increases. This is due to the optimized placement of each antenna in the FAs scheme, which enhances beamforming gains and thereby facilitates more efficient task offloading.

The relationship between the TCD and the edge computing capacity f_{total} under various algorithms is demonstrated in Fig. 5 with $M = 10$. This further validates the advantages of utilizing FAs, particularly when the edge computing capacity is sufficient. Evidently, TCD decreases as edge computing resources increase and eventually stabilizes. When f_{total} is relatively small, local computation delay is the dominant factor. In contrast, with a sufficiently large edge computing capacity, the transmission delay for task offloading by GUs and SU becomes the primary contributing factor.

Fig. 6 depicts the TCD versus the edge computing resource f_{total} for different noise power levels σ^2 and satellite–to-UAV propagation delays T_o. The TCD decreases monotonically with increasing f_{total} and gradually saturates. For a fixed noise power, a larger T_o consistently leads to a higher TCD with almost identical curve shapes. For a fixed T_o, the curves with $\sigma^2 = -70$ dBm lie above those with $\sigma^2 = -80$ dBm and -90 dBm, reflecting the degradation of uplink channel

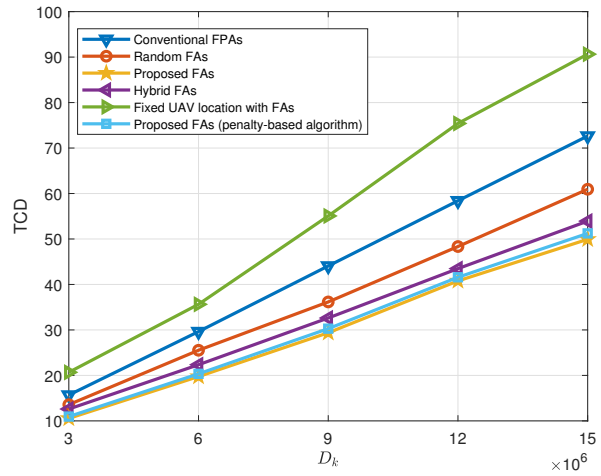

Fig. 7. TCD performance versus the computational task size of users with different algorithms under $M = 16$.

quality and longer offloading delays. Moreover, the TCD gap between -70 dBm and -80 dBm is slightly larger than that between -80 dBm and -90 dBm. Furthermore, error bars are plotted on the curve with $\sigma^2 = -80$ dBm and $T_o = 10$ ms to capture the variation of TCD at 500 random GU locations. Their magnitudes are clearly smaller than the separations between different parameter curves, indicating that the proposed FA-assisted scheme is reasonably robust to the spatial randomness of user locations, while the sensitivity to such randomness becomes relatively higher when computation and communication delays are of comparable importance.

Next, Fig. 7 shows the relationship between TCD and the task size of edge computing users with $M = 16$. For simplicity, the task sizes of GUs and SU are assumed to be identical and are collectively denoted as D_k. The TCD of all schemes increases with D_k, as a larger task size leads to a longer completion time, regardless of whether it is processed locally or offloaded. As D_k increases, the performance gap

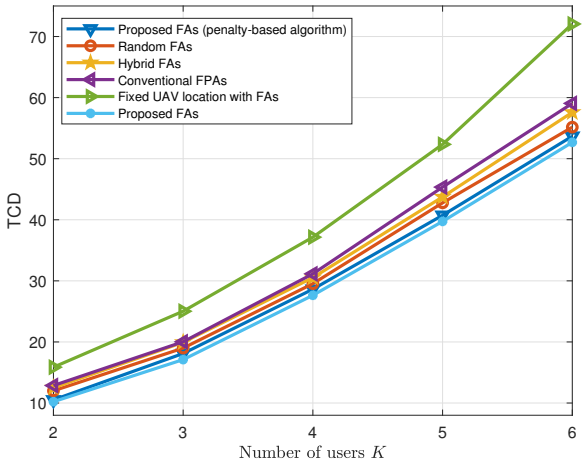

Fig. 8. TCD performance versus the number of edge computing users K.

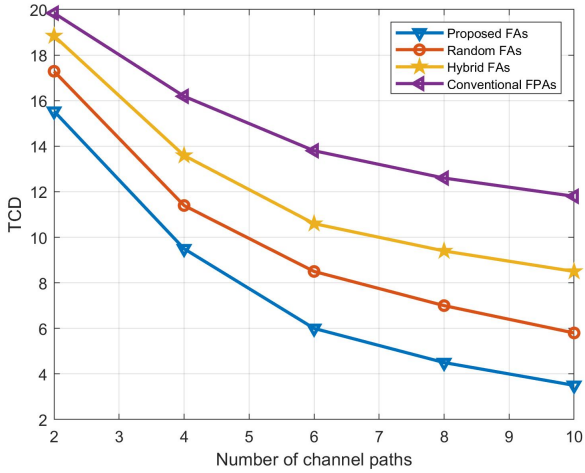

Fig. 9. TCD performance versus the number of channel paths L.

between the proposed FAs scheme and other schemes gradually widens. This indicates that when the task size is large, the proposed FAs scheme can more effectively reduce task offloading latency, further demonstrating the advantages of optimized antenna placement in edge computing. Moreover, relative to the baseline with fixed UAV location and FAs, the proposed scheme exhibits consistently lower TCD and a smaller growth rate with respect to D_k, underscoring the necessity of jointly optimizing the UAV position together with the other design variables. In addition, compared with the penalty-based algorithm for solving the receive beamforming, our proposed method maintains a slight yet consistent advantage across the entire range of D_k.

To evaluate the impact of the number of edge computing users on the TCD performance, we provide comparison results as indicated in Fig. 8. It is observed that the TCD performance of all schemes increases as the number of users K increases. The proposed FA scheme outperforms the conventional FPA scheme, further demonstrating the superiority of FA over FPA in the MEC-SAGIN system. Specifically, the schemes with FAs, Hybrid FAs, and random FAs positioning achieve approximately 11.9%, 9.32%, and 4.7% TCD gains, respectively, compared to the FPAs scheme. In addition, fixing the UAV location leads to larger TCD, with an increasing gap relative to the proposed FAs as K grows. Compared to the conventional FPAs scheme, the FAs scheme can dynamically adjust antenna positions and optimize task offloading strategies, thereby mitigating the challenges posed by limited computational and communication resources in multi-user environments. As the number of users K increases, the performance advantage of the FAs scheme becomes more pronounced, further validating its superiority in high-user-density scenarios.

Fig. 9 illustrates the relationship between the TCD and the number of channel paths of GUs and SU, i.e. L. For simplicity, we set $L_r = L_t = L$. The TCD of all schemes decreases as L increases since a higher number of channel paths enables greater multi-path diversity and facilitates more efficient offloading strategies, thereby reducing TCD. Moreover, the

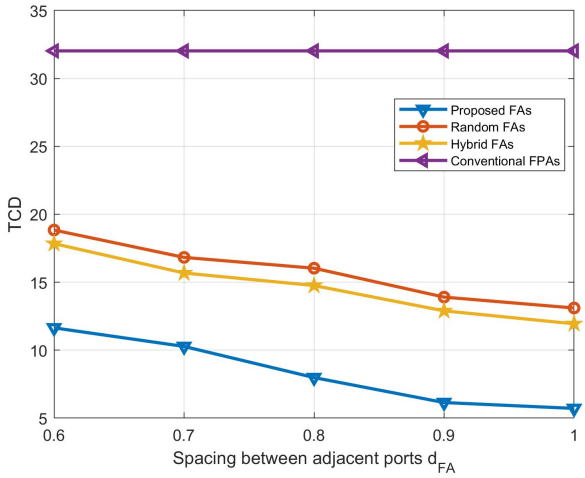

Fig. 10. TCD performance versus the spacing d_{FA}.

performance gap between the proposed FAs scheme and the other two schemes increases with L, further validating the effectiveness of our proposed algorithm.

Finally, we compare the TCD performance of four different schemes under varying port spacing in Fig. 10. It is observed that, except for the conventional FPAs scheme, the TCD of all FA-based schemes decreases as the adjacent port spacing d_{FA} increases. This indicates that enlarging the port spacing mitigates inter-antenna interference, thereby enhancing channel quality and improving task offloading efficiency. As d_{FA} increases, the TCD of the random FAs, the proposed FAs design, and the Hybrid FAs schemes initially decrease and then converge to a constant value. This phenomenon suggests that the optimization of antenna spacing has an upper limit, and only within a certain range can achieve the best system performance.

V. Conclusion

In this paper, we investigated task offloading and wireless resource management in an FA-assisted MEC-SAGIN system.

To minimize the maximum TCD among edge computing users, we jointly optimized the offloading ratio, CPU frequency, FA port selection, UAV location, and receive beamforming. Simulation results demonstrated that the proposed FA design achieved significantly lower TCD than conventional FPAs and random-port schemes. These findings indicate that integrating FA into MEC-SAGIN can substantially enhance channel conditions and improve overall offloading and computation efficiency.

As our future work, an energy-minimization based design will be conceived for FA-assisted MEC-SAGIN systems that explicitly accounts for practical FA hardware constraints and scalable multi-UAV architectures. We will also investigate reliability-oriented, secure, and privacy-preserving offloading mechanisms tailored to FA-assisted MEC-SAGIN deployments.

REFERENCES

[1] T. Mai, H. Yao, N. Zhang, L. Xu, M. Guizani, and S. Guo, "Cloud mining pool aided blockchain-enabled internet of things: An evolutionary game approach," *IEEE Trans. Cloud Comput.*, vol. 11, no. 1, pp. 692–703, 2023.

[2] Y. Zhu, H. Yao, T. Mai, W. He, N. Zhang, and M. Guizani, "Multiagent reinforcement-learning-aided service function chain deployment for internet of things," *IEEE Internet Things J.*, vol. 9, no. 17, pp. 15 674–15 684, 2022.

[3] W. Shi, J. Cao, Q. Zhang, Y. Li, and L. Xu, "Edge computing: Vision and challenges," *IEEE Internet Things J.*, vol. 3, no. 5, pp. 637–646, 2016.

[4] C. Qiu, H. Yao, C. Jiang, S. Guo, and F. Xu, "Cloud computing assisted blockchain-enabled internet of things," *IEEE Trans. Cloud Comput.*, vol. 10, no. 1, pp. 247–257, 2022.

[5] P. Mach and Z. Becvar, "Mobile edge computing: A survey on architecture and computation offloading," *IEEE Commun. Surv. & Tut.*, vol. 19, no. 3, pp. 1628–1656, 2017.

[6] X. Chen, L. Jiao, W. Li, and X. Fu, "Efficient multi-user computation offloading for mobile-edge cloud computing," *IEEE/ACM Trans. Networking*, vol. 24, no. 5, pp. 2795–2808, 2016.

[7] Y. Mao, J. Zhang, and K. B. Letaief, "Dynamic computation offloading for mobile-edge computing with energy harvesting devices," *IEEE J. Sel. Areas Commun.*, vol. 34, no. 12, pp. 3590–3605, 2016.

[8] T. Taleb, K. Samdanis, B. Mada, H. Flinck, S. Dutta, and D. Sabella, "On multi-access edge computing: A survey of the emerging 5G network edge cloud architecture and orchestration," *IEEE Commun. Surv. & Tut.*, vol. 19, no. 3, pp. 1657–1681, 2017.

[9] S. Wang, X. Zhang, Y. Zhang, L. Wang, J. Yang, and W. Wang, "A survey on mobile edge networks: Convergence of computing, caching and communications," *IEEE Access*, vol. 5, pp. 6757–6779, 2017.

[10] T. X. Tran, A. Hajisami, P. Pandey, and D. Pompili, "Collaborative mobile edge computing in 5g networks: New paradigms, scenarios, and challenges," *IEEE Commun. Mag.*, vol. 55, no. 4, pp. 54–61, 2017.

[11] J. Liu, Y. Shi, Z. M. Fadlullah, and N. Kato, "Space-air-ground integrated network: A survey," *IEEE Commun. Surv. & Tut.*, vol. 20, no. 4, pp. 2714–2741, 2018.

[12] C. Zhou, W. Wu, H. He, P. Yang, F. Lyu, N. Cheng, and X. Shen, "Deep reinforcement learning for delay-oriented IoT task scheduling in SAGIN," *IEEE Trans. Wireless Commun.*, vol. 20, no. 2, pp. 911–925, 2021.

[13] N. Cheng, F. Lyu, W. Quan, C. Zhou, H. He, W. Shi, and X. Shen, "Space/aerial-assisted computing offloading for IoT applications: A learning-based approach," *IEEE J. Sel. Areas Commun.*, vol. 37, no. 5, pp. 1117–1129, 2019.

[14] N. Kato, Z. M. Fadlullah, F. Tang, B. Mao, S. Tani, A. Okamura, and J. Liu, "Optimizing space-air-ground integrated networks by artificial intelligence," *IEEE Wireless Commun.*, vol. 26, no. 4, pp. 140–147, 2019.

[15] B. Cao, J. Zhang, X. Liu, Z. Sun, W. Cao, R. M. Nowak, and Z. Lv, "Edge–cloud resource scheduling in space–air–ground-integrated networks for internet of vehicles," *IEEE Internet Things J.*, vol. 9, no. 8, pp. 5765–5772, 2022.

[16] M. Jia, J. Wu, Q. Guo, and Y. Yang, "Service-oriented SAGIN with pervasive intelligence for resource-constrained users," *IEEE Network*, vol. 38, no. 2, pp. 79–86, 2024.

[17] B. Chen, N. Li, Y. Li, X. Tao, and G. Sun, "Energy efficient hybrid offloading in space-air-ground integrated networks," in *IEEE Wireless Commun. and Netw. Conf. (WCNC)*, 2022, pp. 1319–1324.

[18] S. Yoo, S. Jeong, J. Kim, and J. Kang, "Cache-assisted mobile-edge computing over space–air–ground integrated networks for extended reality applications," *IEEE Internet Things J.*, vol. 11, no. 10, pp. 18 306–18 319, 2024.

[19] J. Du, J. Wang, A. Sun, J. Qu, J. Zhang, C. Wu, and D. Niyato, "Joint optimization in blockchain- and MEC-enabled space–air–ground integrated networks," *IEEE Internet Things J.*, vol. 11, no. 19, pp. 31 862–31 877, 2024.

[20] Y. Pang, D. Wang, D. Wang, L. Guan, C. Zhang, and M. Zhang, "A space-air-ground integrated network assisted maritime communication network based on mobile edge computing," in *IEEE World Congr. on Services (SERVICES)*, 2020, pp. 269–274.

[21] S. Yoo, S. Jeong, J. Kim, and J. Kang, "Cache-assisted mobile-edge computing over space–air–ground integrated networks for extended reality applications," *IEEE Internet Things J.*, vol. 11, no. 10, pp. 18 306–18 319, 2024.

[22] Z. Hu, F. Zeng, Z. Xiao, B. Fu, H. Jiang, H. Xiong, Y. Zhu, and M. Alazab, "Joint resources allocation and 3D trajectory optimization for UAV-enabled space-air-ground integrated networks," *IEEE Trans. Veh. Technol.*, vol. 72, no. 11, pp. 14 214–14 229, 2023.

[23] Y. Zhang, J. Wang, Q. Li, J. Chen, H. Feng, and S. He, "Joint communication, sensing, and computing in space–air–ground integrated networks: System architecture and handover procedure," *IEEE Veh. Technol. Mag.*, vol. 19, no. 2, pp. 70–78, 2024.

[24] J. Li, Y. Shi, C. Dai, C. Yi, Y. Yang, X. Zhai, and K. Zhu, "A learning-based stochastic game for energy efficient optimization of UAV trajectory and task offloading in space/aerial edge computing," *IEEE Trans. Veh. Technol.*, pp. 1–16, 2025.

[25] W. Zhu, X. Deng, J. Gui, H. Zhang, and G. Min, "Cost-effective task offloading and resource scheduling for mobile edge computing in 6G space-air-ground integrated network," *IEEE Internet Things J.*, pp. 1–1, 2025.

[26] K.-K. Wong, K.-F. Tong, Y. Zhang, and Z. Zhongbin, "Fluid antenna system for 6G: When Bruce Lee inspires wireless communications," *Electron. Lett.*, vol. 56, no. 24, pp. 1288–1290, 2020.

[27] K.-K. Wong, W. K. New, X. Hao, K.-F. Tong, and C.-B. Chae, "Fluid antenna system—part I: Preliminaries," *IEEE Commun. Lett.*, vol. 27, no. 8, pp. 1919–1923, 2023.

[28] K.-K. Wong, A. Shojaeifard, K.-F. Tong, and Y. Zhang, "Fluid antenna systems," *IEEE Trans. Wireless Commun.*, vol. 20, no. 3, pp. 1950–1962, 2020.

[29] W. K. New, K.-K. Wong, H. Xu, C. Wang, F. R. Ghadi, J. Zhang, J. Rao, R. Murch, P. Ramírez-Espinosa, D. Morales-Jimenez *et al.*, "A tutorial on fluid antenna system for 6G networks: Encompassing communication theory, optimization methods and hardware designs," *IEEE Commun. Surv. & Tut.*, 2024.

[30] K.-K. Wong and K.-F. Tong, "Fluid antenna multiple access," *IEEE Trans. Wireless Commun.*, vol. 21, no. 7, pp. 4801–4815, 2021.

[31] H. Xu, G. Zhou, K.-K. Wong, W. K. New, C. Wang, C.-B. Chae, R. Murch, S. Jin, and Y. Zhang, "Channel estimation for FAS-assisted multiuser mmWave systems," *IEEE Commun. Lett.*, vol. 28, no. 3, pp. 632–636, Mar. 2024.

[32] H. Xu, K.-K. Wong, W. K. New, F. R. Ghadi, G. Zhou, R. Murch, C.-B. Chae, Y. Zhu, and S. Jin, "Capacity maximization for FAS-assisted multiple access channels," *IEEE Trans. Commun.*, 2024.

[33] W. Ma, L. Zhu, and R. Zhang, "Multi-beam forming with movable-antenna array," *IEEE Commun. Lett.*, vol. 28, no. 3, pp. 697–701, 2024.

[34] L. Zhu, W. Ma, and R. Zhang, "Movable-antenna array enhanced beamforming: Achieving full array gain with null steering," *IEEE Commun. Lett.*, vol. 27, no. 12, pp. 3340–3344, 2023.

[35] K.-K. Wong, K.-F. Tong, Y. Chen, and Y. Zhang, "Fast fluid antenna multiple access enabling massive connectivity," *IEEE Commun. Lett.*, vol. 27, no. 2, pp. 711–715, 2023.

[36] W. Mei, X. Wei, B. Ning, Z. Chen, and R. Zhang, "Movable-antenna position optimization: A graph-based approach," *IEEE Wireless Commun. Lett.*, vol. 13, no. 7, pp. 1853–1857, 2024.

[37] P. Chen, Y. Yang, B. Lyu, Z. Yang, and A. Jamalipour, "Movable antenna-enhanced wireless powered mobile edge computing systems," *IEEE Internet Things J.*, pp. 1–1, 2024.

[38] Y. Zuo, J. Guo, B. Sheng, C. Dai, F. Xiao, and S. Jin, "Fluid antenna for mobile edge computing," *IEEE Commun. Lett.*, vol. 28, no. 7, pp. 1728–1732, 2024.

[39] L. Zhu, X. Pi, W. Ma, Z. Xiao, and R. Zhang, "Dynamic beam coverage for satellite communications aided by movable-antenna array," *IEEE Trans. Wireless Commun.*, pp. 1–1, 2024.

[40] Y. Chen, M. Chen, H. Xu, Z. Yang, K.-K. Wong, and Z. Zhang, "Joint beamforming and antenna design for near-field fluid antenna system," *IEEE Wireless Commun. Lett.*, vol. 14, no. 2, pp. 415–419, 2025.

[41] L. Zhu, W. Ma, B. Ning, and R. Zhang, "Movable-antenna enhanced multiuser communication via antenna position optimization," *IEEE Trans. Wireless Commun.*, vol. 23, no. 7, pp. 7214–7229, 2024.

[42] S. Boyd and L. Vandenberghe, *Convex optimization*. Cambridge university press, 2004.